axonal spheroids is not topographically correlated with the sites of neuronal loss that preferentially involve cerebellar Purkinje cells, VPL–VPM thalamic neurons, and GABAergic interneurons (Higashi et al., 1993; March et al., 1997; Tanaka et al., 1988; Yamada et al., 2001). On the other hand, recent studies have demonstrated that the degeneration of axons precedes that of neuronal cell body, suggesting the occurrence of dying back processes (Ong et al., 2001). This raises the possibility that spheroid formation may represent a unique form of distal axonopathy in which the terminal portion of axons and presynaptic axon terminals are preferentially affected, which could result in synaptic dysplasia and differential vulnerability of axons depending on their length.

To study on the pathogenetic role of spheroid formation in neurodegeneration in NP-C, we focused on the sites of termination of central processes of dorsal root ganglion (DRG) neurons. The gracile nuclei of the medulla oblongata, one of the principal sites of termination of lengthy myelinated axons derived from large-sized lumbosacral DRG neurons, are known for the development of neuroaxonal dystrophy (NAD) (Jellinger, 1973). NAD, unlike nonspecific axonal swelling, is characterized by unique ultrastructural features such as accumulation of smooth membrane, tubulo-membranous aggregates, and a few neurofilaments (Seitelberger, 1986), and develops as a function of normal aging in rodents as well as humans (Fujisawa and

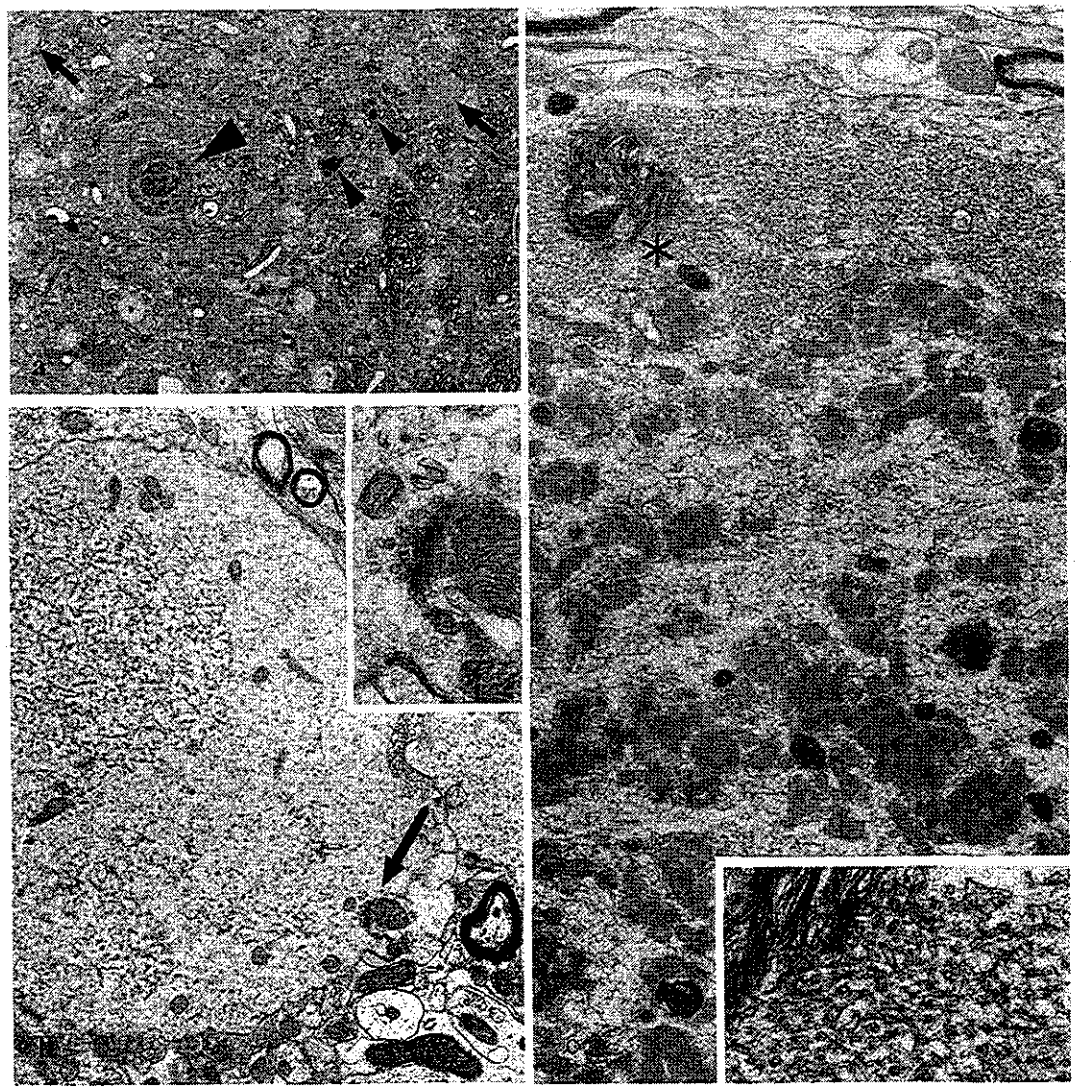

Fig. 1. The gracile nuclei of normal aging mouse (16-month-old, Balb/c). (a) Light microscopy revealed a varied appearance of neuroaxonal dystrophy in the nuclei. Most dystrophic elements are spherical to oval in shape and showed granular (arrowheads) or homogenous texture (arrows). (Epon semithin section stained with Toluidine blue (×265)). (b) This electron micrograph illustrates a dystrophic axon indicated with a curved arrow in a. The enlarged presynaptic terminal is electron lucent and is interspersed with many vesicles and a tubulo-vesicular network (×6900). (Inset) Higher magnification of the area indicated with an arrow showing a synaptic junction (×23,000). (c) This electron micrograph illustrates the spheroid indicated with a large arrowhead in a. The light microscopic granular appearance of dystrophic axons corresponds to clusters of degenerated mitochondria, interspersed neurofilaments, and dense bodies (×9800). (Inset) A higher magnification of the periphery of the NAD indicated with * in a, showing tubulo-vesicular structures (×29,500).

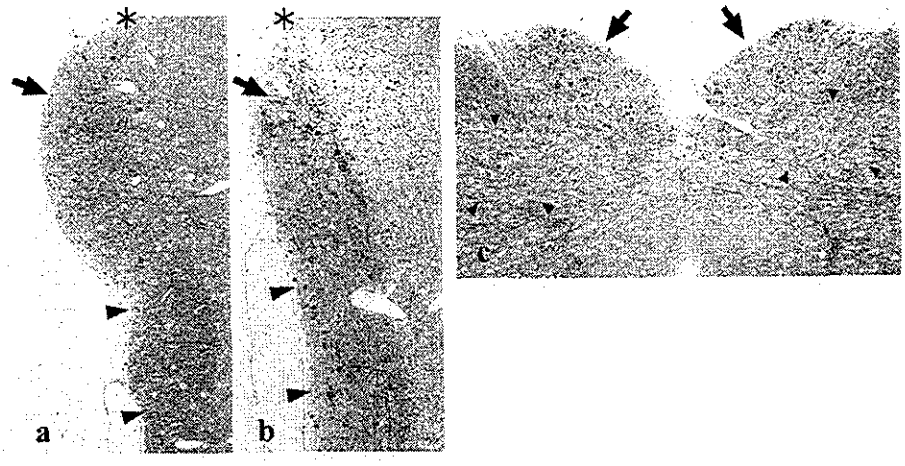

Fig. 2. Longitudinal (a and b) and axial (c) sections of the dorsal column nuclei at 3 weeks (a) and 6 weeks (b and c) of age of NP-C mice. (a and b) At 3 weeks, dot-like axonal spheroids (stained dark with Toluidine blue) could be recognized exclusively in the gracile nuclei (thick arrow) and not in the gracile fasciculus (arrowheads). At 6 weeks, the spheroids are seen not only in the nucleus but also in the proximal portion of the gracile fasciculus, and they increased in density and in individual size. Asterisks (*) indicate the location of the obex. (c) A representative axial section of the medulla oblongata from a 6 – week-old NP-C mouse cut at the level of the obex showing the pair of dorsal column nuclei: thick arrows indicate the adjacent gracile nuclei, and the arrowheads the adjacent cuneate nuclei. Even in this low magnification, the massive involvement of the gracile nuclei by axonal spheroids is evident. (Epon semithin section stained with Toluidine blue. a and b, × 60; c, × 40.)

Shiraki, 1978). On the other hand, the cuneate nuclei with shorter length of afferents compared with the gracile are far less prone to develop neuroaxonal dystrophy than the gracile despite both nuclei, collectively known as dorsal column nuclei, having the same physiological functions subserving sensory transmission of tactile and proprioceptive sensations from the upper (cuneate) and the lower (gracile) extremities to the sensory thalamus. In the spinal cord, the substantia gelatinosa of the spinal dorsal horn (lamina II) is the predominant site of termination of small-sized DRG neurons, largely subserving pain and temperature sensation. Unlike dorsal column nuclei, which receive exclusively myelinated fiber afferents, the substantia gelatinosa receives mostly unmyelinated afferents (Giuffrida and Rustioni, 1992; Ralston and Ralston, 1979; Rustioni and Sotelo, 1974). Thus, given this inherent propensity for DRG neurons to develop axonal dystrophy and their marked variance in the length and size of central processes, the study of projections of DRG neurons should provide an important clue for the understanding of the mechanism of neurodegeneration in NP-C.

In this study, we employed electron microscopy and morphometric techniques to define structural alterations of the central processes of DRG neurons of Balb/c npc^{nih}, an authentic murine model of human NP-C with identical genetic and chemical defects. We found that the central processes of DRG neurons of the NP-C model mouse are affected in a length-dependent manner; the changes being by far the most dramatic in the gracile nuclei compared to the cuneate and the dorsal horn on the spinal cord, and they were associated with axonal loss and a strikingly early development of axonal dystrophy identical to that seen in the aging gracile nucleus.

Material and methods

Animals

A colony of Balb/c npc^{nih} mutant mice has been maintained and the genotype of each mouse was determined by PCR using genomic DNA isolated from a small piece of the tail as described (Loftus et al., 1997). Thirteen affected mice of 3, 6, and 9 weeks of age ($n \geq 4$ each) and 15 age-matched control mice ($n \geq 4$) were used in this study. Moreover, to access the effect of aging of the gracile NAD in Balb/c mice, 4- and 5 ($n = 1$ each)-, 10 ($n = 2$)-, and 16-month-old mice ($n = 2$) were also studied.

Table 1
The density of axonal spheroids in NPC mice

Age (in weeks)		Diameter (μm)		
		≥5	≥10	≥15
3 ($n = 4$)	Gracile	5.0 ± 1.4 (8.8)	0	0
	Cuneate	0	0	0
6 ($n = 4$)	Gracile	60.2 ± 19.9	13.5 ± 8.1	1.5 ± 1.3 (17.3)
	Cuneate	12.5 ± 3.1	1.5 ± 1.3 (12.7)	0
9 ($n = 5$)	Gracile	107.2 ± 13.8	38.0 ± 7.5	10.4 ± 2.9 (33.9)
	Cuneate	30.8 ± 8.4	4.2 ± 1.3	0.4 ± 0.5 (19.3)

The axonal spheroids (greater than 5 μm in diameter) were identified in a selected rectangle-shaped area (81,000 μm^2) in the gracile and cuneate nuclei in which the density of spheroid was greatest. The numbers in the parentheses indicate the diameter (μm) of the largest spheroid in the series. All assessments were made on a single axial section at the level of obex. In age-matched controls, no spheroids could be found.

Light and electron microscopy

Animals were anesthetized by sodium pentobarbital solution (Dinabot) and perfused transcardially with heparinized PBS followed by freshly prepared 4% paraformaldehyde containing 0.5% glutaraldehyde in 0.1 M phosphate buffer. The brain and the spinal cord with attached lumbar dorsal root ganglia (DRGs) were resected

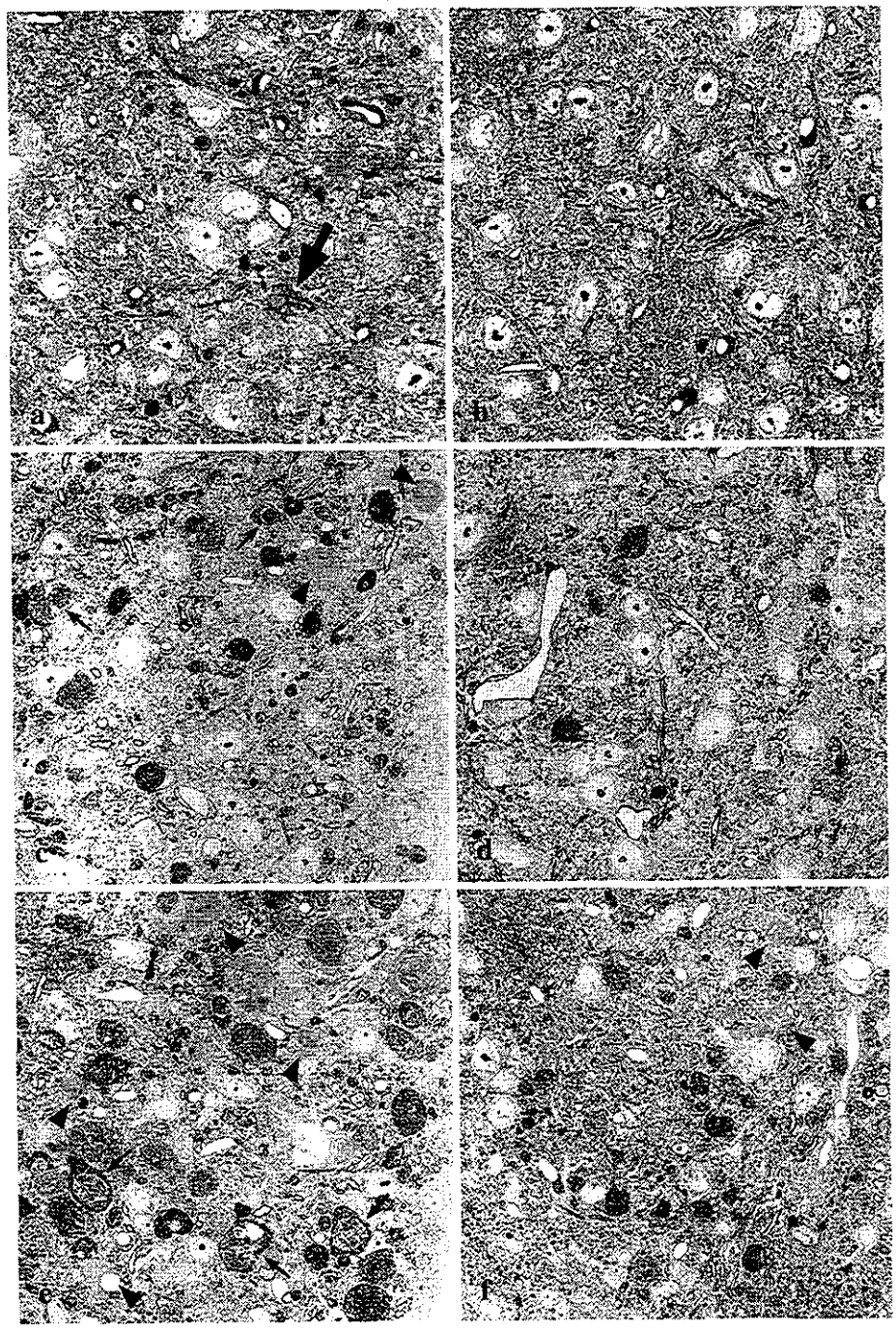

Fig. 3. Light microscopy of the dorsal column nuclei at 3-, 6-, and 9-week-old NP-C mice. In the left column (a, c, and e) are representative pictures from the gracile nuclei at 3, 6, and 9 weeks, respectively, and at the right column (b, d, and e) are those from the adjacent cuneate nuclei. In the gracile nuclei, the progressive increase in the size and the density of axonal spheroids is evident with increasing age especially between 6 and 9 weeks (c and e). At 3 weeks, the spheroids only have a granulated appearance. At 6 and 9 weeks, axonal spheroids with a granular appearance often have a laminar distribution (arrows in c and e). In addition, axonal spheroids with a homogenous texture with or without coexisting granular aggregates are also seen (arrowheads in c and e). Compared with gracile nucleus, the cuneate nuclei (b, d, and f) revealed strikingly fewer spheroids, although both granular and homogenous forms (arrowheads in f) are also recognized. Note the apparently degenerated shrunken neuron (arrow in a) in gracile nuclei of 3-week-old NP-C mice, which was rarely seen and is unlikely to represent fixation artifacts. (Epon semithin section stained with Toluidine blue, × 340.)

and postfixed overnight in the same fixative. The medulla oblongata was cut through the axial plane passing the obex (n = 4 or 5) (Fig. 2c) or cut longitudinally through the gracile nucleus and fasciculus (n = 1 or 2). Tissue blocks of the VPL–VPM thalamus, spinal cord at the level of C2, mid-thoracic and L4, and DRGs were also cut. The dorsal and ventral roots were sampled immediately proximal to the L4 and L5 DRG on the right side; their identification could be easily made by dissecting rostrally from the sciatic nerve. The tissue blocks were postfixed in 1% osmium tetroxide, dehydrated in a graded ethanol series, and then embedded in Epon 812 (Polyscience, Warrington, PA). Sections (1 μm thick) were cut and stained with 1% toluidine blue. For ultrastructural studies, ultrathin sections from selected blocks were cut and stained with uranyl acetate and lead citrate. They were examined with a Hitachi HS-9 or Joel 1200 electron microscope.

Morphometry

The image analysis program Macscope™ (Mitani Co. Fukui, Japan) was used. Digital photo images were obtained with a light microscope and an attached CCD camera interfaced with a computer. The numbers of axonal spheroids with diameter larger than 5 μm were counted with a final magnification on the display screen at ×2000 of a rectangle-shaped area of 81,000 μm^2 in the location in which the density of spheroids is greatest in the gracile and cuneate nuclei of affected mice for each age group ($n \geq 4$). For quantitation of nerve root lesions, the total number of myelinated fibers was counted and the total fascicular area was measured from the pair of ventral L4 + 5 and dorsal L4 + 5 roots, respectively. Statistical analysis was performed using Student's non-paired t tests.

Results

Light and electron microscopy of the gracile nuclei of normal aging mice

In the control gracile nuclei of 3, 6, and 9 weeks (n = 4–5) and 5 months (n = 2) of age Balb/c mice, axonal spheroids were not identified. At 11 and 14 months (n = 2 each), the appearance of spheroids was a constant feature in the gracile nucleus, a finding that was more evident at 14 months of age. The dystrophic axons were spherical in shape and exhibited a granular, homogenous, or mixed appearance (Fig. 1a). Ultrastructurally, dystrophic axonal swellings revealed an admixture of mitochondria, vesicles, dense bodies, neurofilaments, and tubular networks (Figs. 1b and c). Occasionally, synaptic contact with dendrites could be recognized, clearly indicating the presynaptic nature of these dystrophic elements (Fig. 1b).

Light microscopy of NP-C mouse

The dorsal column nuclei and the spinal dorsal horn

When examined on longitudinal sections of the gracile nuclei and fasciculus, the spheroids could be recognized only in the gracile nuclei proper at 3 weeks (Fig. 2a). By 6 and 9 weeks, they could also be seen in the proximal portion of the gracile fasciculus (Fig. 2b). Compared with the gracile nuclei, the cuneate nuclei contained fewer spheroids that started to appear at 6 weeks (Fig. 2c). The size and the density of the axonal spheroids in the gracile nucleus increased dramatically between 6 and 9 weeks (Table 1).

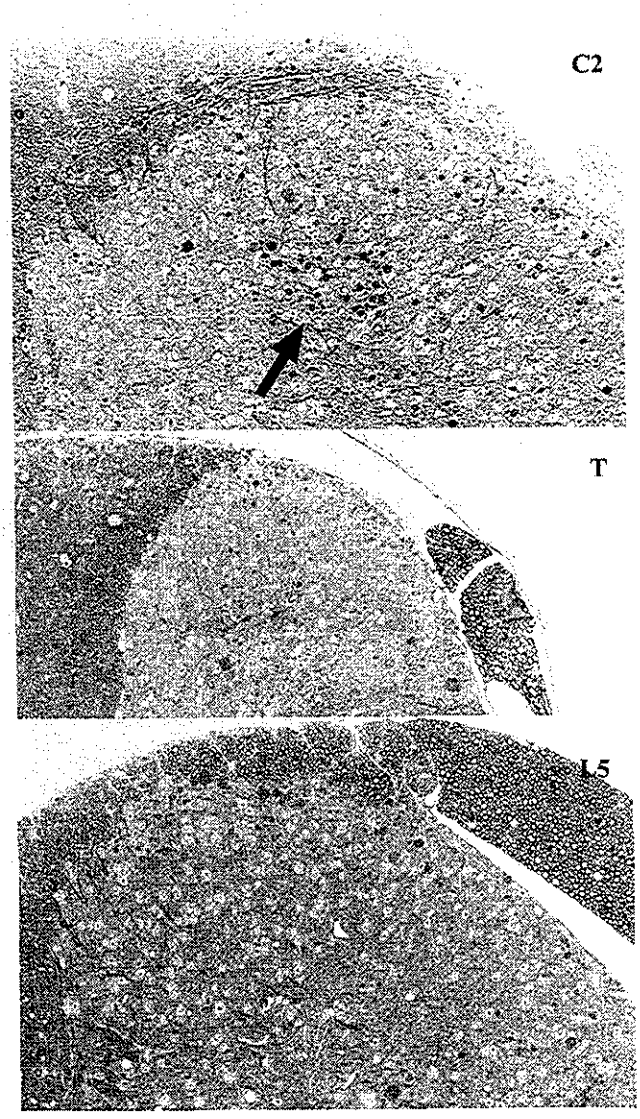

Fig. 4. Representative photographs of the spinal dorsal horn at the level of cervical (C2), middle thoracic (T), and lumbar (L5) spinal segments from a 9-week-old NP-C mouse. Axonal spheroids are frequently seen in lamina I and outer portion of lamina II (substantia gelatinosa) as well as lamina III and IV. The dramatic appearance of axonal spheroids in lamina III (arrow) was a conspicuous feature in upper cervical spinal cord segments compared with thoracic and lumbar segments. (Epon semithin sections stained with Toluidine blue, × 1100.)

Morphologically, three forms could be recognized; one showing granular, often laminar arrangement, the other showing homogeneous density containing lucent clefts, and a mixture of the two (Fig. 3). Intracytoplasmic inclusions were also evident in the neuronal perikarya, certain glial cells, and endothelial cells. Reactive astrocytes and infiltration of foamy macrophages were apparent at 6 weeks and in greater number at 9 weeks.

In the spinal dorsal horn, only a few spheroids could be recognized at 3 weeks at lamina III. At 6 and 9 weeks, they became increased in number and size, and could be recognized in the entire lamina (I–IV), although they were espe-

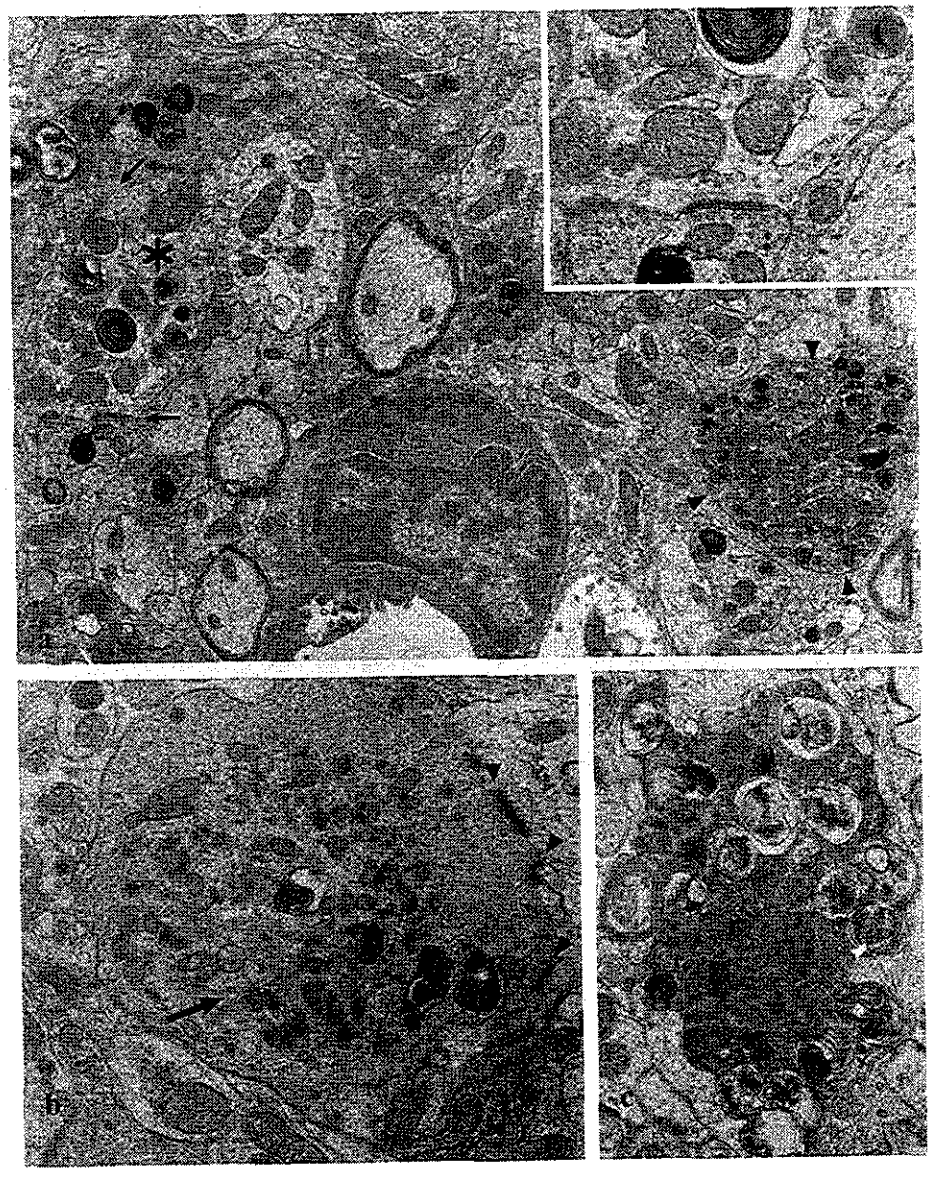

Fig. 5. Electron microscopy of the gracile nucleus of NP-C mouse. (a) Low power view of the gracile nuclei at 3 weeks. An axonal spheroid (arrowheads) is seen studded with mitochondria and dense bodies. Typical lamellated inclusions characteristic of NP-C are seen in a dendrite (*) that forms synapses with two axon terminals (arrows) containing dense bodies and mitochondria. (Inset) Higher magnification of the area indicated with a thin arrow showing the synaptic junction. Also note the presence of inclusions in capillary endothelial cell (× 7800). (b) This electron micrograph shows dystrophic axon terminals of 6-week-old NP-C mice. In addition to an increased number of synaptic vesicles, mitochondria and dense bodies of varied size, tubular structures are seen in the center (arrow). Three synaptic junctions are formed on its surface (arrowheads) (× 16,400). (c) This electron micrograph illustrates a degenerating presynaptic axon terminal at 6 weeks, showing shrunken electron-dense cytoplasm filled with dense amorphous materials (× 13,900). (d) This electron micrograph illustrates typical dystrophic axons that had a lamellar appearance by light microscopy. The core of the dystrophic axon largely consisted of an accumulation of mitochondria, while its periphery contains more filamentous material and vesicles. Six-week-old NP-C mouse (× 7000). (Inset) Higher magnification of the area indicated with arrow revealing several synaptic junctions between the dystrophic axon and dendrite (× 8000). (e) This electron micrograph illustrates the typical ultrastructure of the dystrophic axons with homogeneous appearance by light microscopy. An enlarged dystrophic axon terminal (ax) filled with tubulomembranous aggregates, vesicles, and filamentous materials is in synaptic contact with a dendrite (den). The latter contains lamellated inclusions characteristic of NP-C (arrow). Note a filopodic process budding from the enlarged dystrophic axon terminal (arrowheads). Nine-week-old NP-C mouse (× 9000).

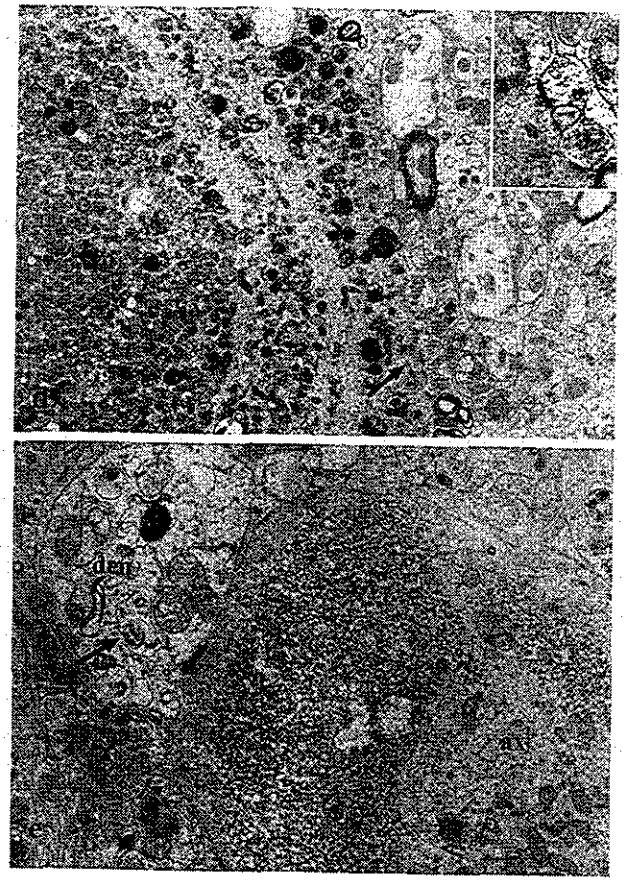

Fig. 5 (*continued*).

cially conspicuous in lamina I and III (Fig. 4). Among the three levels of spinal cord segments examined (C2, mid-thoracic and L5), their appearance was consistently most dense at the C2 segment, probably reflecting the unique cytoarchitectural features of the upper cervical spinal cord (Webster and Kemplay, 1978). The axonal spheroids were generally granular in light microscopic appearance, though occasionally, features of well-developed axonal dystrophy could be recognized.

Ultrastructural observations of dorsal column nuclei and the spinal dorsal horn of the NP-C mice with special attention to the synaptic junctions

At 3 weeks, well-developed synaptic junctions characteristic of gracile nuclei could be easily identified (Rustioni and Sotelo, 1974). Lamellated inclusions characteristic of NP-C were occasionally found in postsynaptic elements (Fig. 5a). Presynaptic axons contained such inclusions less often, but instead revealed early dystrophic changes (Lampert, 1967) consisting of an increased number of neurofilaments, mitochondria, vesicles, and dense bodies. Large axonal spheroids identified by light microcopy consisted of a massive collection of mitochondria and dense bodies, although synaptic junctions could rarely be found on the surface (Fig. 5a). At 6 weeks, enlarged dystrophic presynaptic terminals and degenerating presynaptic terminals were occasionally found (Figs. 5b and c). The ultrastructural substrate of the light microscopic appearance of an enlarged granular spheroid corresponded to a massive accumulation of mitochondria (Fig. 5d), while those with glassy appearance corresponded to diffuse accumulation of tubulo-membranous structures (Fig. 5e). Other subcellular organelles included neurofilaments, dense bodies, myelin-like figures, and electron-lucent clefts. Synapses could occasionally be found even in spheroids with typical ultrastructural features of neuroaxonal dystrophy (Fig. 5e). These features were ultrastructurally indistinguishable from those seen in aging control mouse gracile nuclei (Figs. 1b and c).

In the substantia gelatinosa of the spinal dorsal horn, dystrophic cell processes containing dense bodies and increased numbers of mitochondria were found at 6 weeks. Characteristically, glomeruli, a morphological signature of primary endings of dorsal root ganglion neurons in the spinal dorsal horn, revealed hypertrophic changes with increased number of vesicles, mitochondria, and dense bodies. Occasionally, tubulo-vesicular profiles could be seen in the enlarged terminal axons composing glomeruli.

Table 2
The result of quantitative study on L4 and 5 spinal nerve roots

Age (weeks)	Animals	Dorsal roots		Ventral roots	
		Total number of myelinated axons	Total fascicular area (hundreds of μm^2)	Total number of myelinated axons	Total fascicular area (hundreds of μm^2)
3	Control (n = 5)	3955 ± 101	538.7 ± 15.9	1828 ± 25.8	452.0 ± 28.5
	NP-C (n = 4)	3561 ± 107**	572.1 ± 17.1	1698 ± 71.3	472.2 ± 28.9
6	Control (n = 5)	4791 ± 136	1018 ± 55.0	1950 ± 60.1	681.2 ± 39.0
	NP-C (n = 4)	4564 ± 235	957.6 ± 48.2	1779 ± 43.5	568.5 ± 32.6
9	Control (n = 5)	4947 ± 72	1233 ± 46.5	1946 ± 53.9	930.5 ± 44.2
	NP-C (n = 5)	4222 ± 77*	871.7 ± 38.3**	1781 ± 13.3**	650.2 ± 24.0**

The L4 and 5 dorsal and ventral spinal nerve roots of the right side were examined in the study (see Materials and methods). Note that there was a significant decrease in myelinated axons in the dorsal roots at 3 and 9 weeks but not at 6 weeks. The decrease at 3 weeks was apparently due to delayed myelination in NP-C mouse. Each figure represents mean ± SEM.

* $P < 0.005$.

** $P < 0.05$.

Quantitative study on spinal dorsal nerve roots

The total number of myelinated axons of combined L4 and 5 dorsal roots increased from 3 to 6 weeks in both controls and NP-C, reflecting an ongoing myelinating process during that period, and reached a plateau at 6 weeks (Table 2). At 3 and 9 weeks, there was a significant difference in the number of myelinated axons between controls and NP-C mice. The difference at 3 weeks probably reflects delayed myelination, which is known to occur in NP-C mice (Higashi et al., 1991). At 9 weeks, there was a statistically more significant ($P < 0.005$) decrease in the number of myelinated axons in NP-C mice compared to age-matched controls with a concordant decrease in the total fascicular area.

Discussion

It has been well established that the development of axonal swellings (spheroids) is one of the cardinal histopathological features of brains of NP-C involving brains of both human and mice (Higashi et al., 1991; Vanier and Suzuki, 1998) along with neuronal storage and neuronal loss, all of which eventually affect the entire CNS. The cerebellum and VPL–VPM thalamus are among the earliest sites of involvement in NP-C, although the underlying mechanism of neurodegeneration is unknown. Recently, it has been demonstrated that axons degenerate earlier than the cell body in NPC mouse brain. Thus, in cerebellar Purkinje cells, axonal spheroids could be recognized in the projections of Purkinje cells to the deep cerebellar nuclei before involvement of the cell bodies (March et al., 1997). Similar observations were made in the cortical pyramidal neurons and the hippocampus (Ong et al., 2001). These findings suggest that spheroid formation involving the axon terminals and not loss of neuronal cell body could account for certain functional abnormalities in NP-C, especially in the early stage of the illness. However, few ultrastructural studies of the presynaptic axon terminals have been available to further elucidate this point. In the present study, we have systematically studied the presynaptic axon terminals of the central processes of DRG neurons of NP-C mouse and found that axonal spheroid most substantially involved lengthy axons projecting to the gracile nuclei compared with shorter axons terminating in the cuneate. Dystrophic axons were much less frequent in the anterior horn of the lumbar spinal cord in which some collaterals of large myelinated axons, also projecting to the gracile nucleus in the dorsal column, subserve a local reflex arc. This strongly suggests that the length of axons determines whether the same neuronal processes develop axonal spheroid either early or late in the disease processes. It is also noteworthy that lamina II of the spinal dorsal horn (substantia gelatinosa) consistently develops fewer axonal spheroids compared to lamina III–IV. Because, unlike lamina III and IV, the substantia gelatinosa receives a majority of unmyelinated fiber afferents, an observation also consistent with the idea that large myelinated axon terminals are more prone to develop spheroids than those of small unmyelinated axons even if the axonal length is the same.

In the present study, it is important to note that axonal spheroids in the gracile nuclei of NP-C mice began to exhibit characteristic ultrastructural features of axonal dystrophy already at 6 weeks, whereas in controls, such features could not be recognized until 5 months. Despite a variety of conditions in which axonal dystrophy is identified, it is regarded as a distinct form of axonopathy that could be separated from simple axonal spheroids by the presence of tubulo-vesicular elements (Schmidt, 1993; Seitelberger, 1986). The occurrence of gracile axonal dystrophy (GAD) with such ultrastructural characteristics has been well known as a function of age in humans (Fujisawa and Shiraki, 1978) and has also been described in certain metabolic and hereditary conditions (Jellinger, 1973; Seitelberger, 1986). Predominant involvement of presynaptic DRG axon terminals is a characteristic feature (Matsuda et al., 1985). Previous ultrastructural studies of aging mouse gracile nuclei demonstrated that only a few axonal swellings are present at 8 months of age, and dystrophic axons were evident at 21–23 months (Johnson et al., 1975). Even in senescence-accelerated (SAM) mice, dystrophic axons could not be detected before 2 months by sensitive NADPH-d histochemistry (Kawamata et al., 1997). In the GAD mutant mouse, in which dying-back type axonal degeneration is a characteristic morphological feature, dystrophic axons were first recognized in the gracile nucleus as early as 40 days of age (Kikuchi et al., 1990; Mukoyama et al., 1989). Thus, the strikingly early appearance of GAD in the NP-C model mouse may make this animal a useful model in studying the cellular mechanisms of neuroaxonal dystrophy. It is known that the formation of GAD can be accelerated in rodents experimentally by peripheral axotomy and in humans by limb amputation (Hachisuka et al., 1989; Ohara et al., 1995, 2000). In the NP-C mouse model, however, the peripheral axons are reportedly well preserved (Higashi et al., 1995), making this an unlikely explanation for the premature appearance of GAD. It may be that the centrally directed axons of DRG neurons of NP-C mouse are more vulnerable than peripherally directed axons; a condition that has been designated as central distal axonopathy syndrome (Thomas et al., 1984).

Our quantitative studies on the spinal dorsal roots indicated that there was a significant axonal loss evident only at 9 weeks ($P < 0.005$), which is well in accord with the accelerated formation of axonal dystrophy observed between 6 and 9 weeks. Because the number of dorsal root axons faithfully reflects the number of DRG neurons, the results strongly suggest that a population of DRG neurons die and disappear during this period. In this regard, the temporal relationship between the neuronal loss of DRG and in sensory thalamus seems worthy of comment. It has been

previously shown that degeneration of VPL–VPM thalamic neurons (but not VL neurons) began by 4–5 weeks of age and progressed gradually to 12–13 weeks (Yamada et al., 2001). The number of VPL–VPL neurons of NPC mice was reduced to one-third the number of those age-matched controls at 6 weeks. In the present study, we found that the lumbar dorsal root axons of NPC mice did not show significant loss at 6 weeks and, even at 9 weeks, the amount of neuronal loss was only 15%, indicating that the degeneration of DRG neurons occurs late and with lesser severity compared with that of sensory thalamus. Therefore, degeneration in sensory thalamus is not likely to represent an ascending trans-synaptic process, more likely reflecting the different underlying mechanism of neurodegeneration between two sites.

Although the physiological role of NP-C-1 protein in neurons has not been fully elucidated, recent evidence indicates that the NP-C-1 protein is involved in transmembrane transport of fatty acids and functions in vesicular redistribution of endocytosed lysosomal cargo (Davies et al., 2000). In NP-C-1-deficient hamster ovary cells, we have shown that the transport of CT–GM1 complexes from early endosomes to the plasma membrane depends on the function of NP-C-1 protein (Sugimoto et al., 2001). In the central nervous system, the NP-C-1 protein is shown to reside in perisynaptic astrocytic processes (Patel et al., 1999), which may suggest that NP-C-1 protein released from the astrocytes may have a direct role in regulating the segmental composition and configuration of distal presynaptic axons. Thus, it is possible that regionally disrupted activity of NP-C-1 protein in NP-C mouse may impair synaptic integrity, thereby causing premature dystrophic changes in presynaptic axon terminals. Alternatively, there are several lines of evidence that suggest that NP-C-1 protein may play an important role in regulating the integrity of axonal transport. The formation of meganeurites and ectopic dendrites represents morphologic sequelae of ganglioside accumulation in neurons including NP-C mice (Vanier and Suzuki, 1998; Zervas et al., 2001). Moreover, axonal spheroids in the brain of NP-C mice have been shown to contain hyperphosphorylated cytoskeletal proteins and are associated with co-accumulation of P25 and cdk5 (Karten et al., 2002). Deregulation of cdk5–P25 in axons may lead to cytoskeletal abnormalities. More recently, it has been demonstrated that transport of endogenously synthesized cholesterol is impaired in NPC-1-deficient neurons (Bu et al., 2002).

Finally, clinical relevance of the premature development of GAD in NP-C seems worthy of consideration. The dorsal column nuclei are sensory relay nuclei subserving tactile and joint position sensation and project to thalamic VPL–VPM nuclei. In NP-C patients and in mutant mouse as well, motor incoordination is one of the cardinal manifestations of the disease (Miyawaki et al., 1982; Morris et al., 1982). Prolongation or absence of the somatosensory evoked cortical potentials following median or peroneal nerve stimulation is commonly found in human NP-C (Higgins et al., 1992). It is quite likely that the failure of proper synaptic connection secondary to synaptic dysplasia we have described could affect proper proprioceptive perception, resulting in sensory ataxia.

In conclusion, the present study has demonstrated an occurrence of length-dependent axonopathy in the central processes of DRG neurons, which is accompanied by the strikingly early appearance of axonal dystrophy in the gracile nucleus and, subsequently, loss of DRG neurons. Further studies are required to elucidate the role of NP-C-1 protein in causing this unique form of axonopathy.

Acknowledgments

We thank Mr. N. Takeda, Department of Clinical Laboratory research, National Chushin-Matsumoto Hospital, and Ms. K. Suzuki, Research Center for Instrumental Analysis, Shinshu University School of Medicine, for their technical assistance and Prof. S. Ikeda, Department of Medicine, Shinshu University School of Medicine, for his support in the electron microscopic study. We also thank Prof. R.E. Schmidt, Department of Pathology (Neuropathology), Washington University School of Medicine, for his invaluable discussion and editorial assistance of the manuscript.

This work was supported by a grant (H12-brain-018) from the Ministry of Health, Labour, and Welfare of Japan.

References

Bu, B., Li, J., Davies, P., Vincent, I., 2002. Deregulation of cdk5, hyperphosphorylation, and cytoskeletal pathology in the Niemann–Pick type C murine model. J. Neurosci. 22, 6515–6525.

Cruz, J.C., Sugii, S., Yu, C., Chang, T.Y., 2000. Role of Niemann–Pick type C1 protein in intracellular trafficking of low density lipoprotein derived-cholesterol. J. Biol. Chem. 275, 4013–4021.

Davies, J.P., Chen, F.W., Ioannou, Y.A., 2000. Transmembrane molecular pump activity of Niemann–Pick C1 protein. Science 290, 2295–2298.

Fujisawa, K., Shiraki, H., 1978. Study of axonal dystrophy. 1. Pathology of the neuropil of the gracile and cuneate nuclei in aging and old rats: a stereological study. Neuropathol. Appl. Neurobiol. 4, 1–20.

Giuffrida, R., Rustioni, A., 1992. Dorsal root ganglion neurons projecting to the dorsal column nuclei of rats. J. Comp. Neurol. 316, 206–220.

Hachisuka, K., Lais, A.C., Dyck, P.J., 1989. Ultrastructural alterations of primary afferent axons in the nucleus gracilis after peripheral nerve axotomy. J. Neuropathol. Exp. Neurol. 48, 413–424.

Higashi, Y., Pentchev, P.G., Murayama, S., Suzuki, K., 1991. Pathology of Niemann–Pick type C: studies of murine mutants. In: Ikuta, F. (Ed.), Neuropathology in Brain Research. Elsevier, Amsterdam, pp. 85–102.

Higashi, Y., Murayama, S., Pentchev, P.G., Suzuki, K., 1993. Cerebellar degeneration in the Nieman–Pick disease type C mouse. Acta Neuropathol. 85, 175–184.

Higashi, Y., Murayama, S., Pentchev, P.G., Suzuki, K., 1995. Peripheral nerve pathology in Niemann–Pick type C mouse. Acta Neuropathol. 90, 158–163.

Higgins, J.J., Patterson, M.C., Dambrosia, J.M., Pikus, A.T., Pentchev, P.G., Sato, S., Brady, R.O., Barton, N.W., 1992. A clinical staging classification for type C Niemann–Pick disease. Neurology 42, 2286–2290.

Jellinger, K., 1973. Neuroaxonal dystrophy: its natural history and related disorders. Prog. Neuropathol. 2, 129–180.

Johnson, J.E., Mehler, W.R., Miquel, J., 1975. A fine structural study of degenerative changes in the dorsal column nuclei of aging mice. Lack of protection by vitamin E. J. Gerontol. 30, 395–411.

Karten, B., Vance, D.E., Campenot, R.B., Vance, J.E., 2002. Cholesterol accumulation in cell bodies, but is decreased in distal axons, of Niemann–Pick C1-deficient neurons. J. Neurochem. 83, 1154–1163.

Kawamata, T., Akiguchi, I., Yagi, H., Irino, M., Sugiyama, H., Akiyama, H., Shimada, A., Takemura, M., Ueno, M., Kitabayashi, T., Ohnishi, K., Seriu, N., Higuchi, K., Hosokawa, M., Takeda, T., 1997. Neuropathological studies of strains of senescence-accelerated mice (SAM) with age-related deficits in learning and memory. Exp. Gerontol. 32, 161–169.

Kikuchi, T., Mukoyama, M., Yamazaki, K., Moriya, H., 1990. Axonal degeneration of ascending sensory neurons in gracile axonal dystrophy mutant mouse. Acta Neuropathol. 80, 145–151.

Lampert, P.W., 1967. A comparative electron microscopic study of degenerating, regenerating, and dystrophic axons. J. Neuropathol. Exp. Neurol. 26, 345–368.

Loftus, S.K., Morris, J.A., Carstea, E.D., Gu, J.Z., Cummings, C., Brown, A., Ellison, J., Ohno, K., Rosenfeld, M.A., Tagle, D.A., Pentchev, P.G., Pavan, W.J., 1997. Murine model of Niemann–Pick C disease: mutation in a cholesterol homeostasis gene. Science 277, 232–235.

March, P.A., Thrall, M.A., Brown, D.E., Mitchell, T.W., Lowenthal, A.C., Walkley, S.U., 1997. GABAergic neuroaxonal dystrophy and other cytopathological alterations in feline Niemann–Pick disease type C. Acta Neuropathol. 94, 164–172.

Matsuda, T., Maeda, M., Morishima, Y., Hashimoto, S., Tateishi, K., Hamaoka, T., Mizuta, H., Takagi, H., 1985. Dystrophic axons in the nucleus gracilis of the normal rat containing cholecystokinin-like immunoreactivity. Acta Neuropathol. 65, 224–234.

Miyawaki, S., Mitsuoka, S., Sakiyama, T., Kitagawa, T., 1982. Sphingomyelinosis, a new mutation in the mouse. J. Hered. 73, 257–263.

Morris, M.D., Bhuvaneswaren, C., Shio, H., Fowker, S., 1982. Lysosomal lipid storage disorder in NCTR-BALB/c mice. Am. J. Pathol. 108, 140–149.

Mukoyama, M., Yamazaki, K., Kikuchi, T., Tomita, T., 1989. Neuropathology of gracile axonal dystrophy (GAD) mouse. An animal model of central distal axonopathy in primary sensory neurons. Acta Neuropathol. 79, 294–299.

Neufield, E.B., Wastney, M., Patel, S., Sureth, S., Cooney, A.M., Dwyer, N.K., et al., 1999. The Niemann–Pick C1 protein resides in a vesicular compartment linked to retrograde transport of multiple lysosomal cargo. J. Biol. Chem. 274, 9627–9635.

Ohara, S., Beaudet, L.N., Schmidt, R.E., 1995. Transganglionic response of GAP-43 in the gracile nucleus to sciatic nerve injury in young and aged rats. Brain Res. 705, 325–331.

Ohara, S., Takahashi, H., Kato, M., Nakamura, T., Tsukada, M., 2000. Transganglionic gracile response following limb amputation in man. Acta Neuropathol. 100, 469–474.

Ong, W.-Y., Kumar, U., Switzer, R.C., Sidhu, A., Suresh, G., Hu, C.-Y., Patel, S.C., 2001. Neurodegeneration in Niemann–Pick type C disease mice. Exp. Brain Res. 141, 218–231.

Patel, S.C., Suresh, S., Kumar, U., Hu, C.Y., Cooney, A., Blanchette-Mackie, E.J., Neufield, E.B., Patel, R.C., Brady, R.O., Patel, Y.C., Pentchev, P.G., Ong, W.Y., 1999. Localization of Nieman–Pick C1 protein in astrocytes: implication for neuronal degeneration in Nieman–Pick type C disease. Proc. Natl. Acad. Sci. U. S. A. 96, 1657–1662.

Pentchev, P.G., Vanier, M.T., Suzuki, K., Patterson, M.C., 1995. Neimann–Pick disease type C. In: Scriver, C.R., Atanbury, J.B., Wyngaarden, J.B., Frederickson, D.S. (Eds.), The Metabolic and Molecular Basis of Inherited Disease. McGraw-Hill, New York, USA, pp. 2625–2639.

Ralston, H.J., Ralston, D.D., 1979. The distribution of dorsal root axons in laminae I, II and III of the Macaque spinal cord: a quantitative electron microscopic study. J. Comp. Neurol. 184, 643–684.

Rustioni, A., Sotelo, C., 1974. Synaptic organization of the nucleus gracilis of the cat. Experimental identification of dorsal root fibers and cortical afferents. J. Comp. Neurol. 155, 441–468.

Schmidt, R.E., 1993. Neuroaxonal dystrophy in aging rodent and humans sympathetic autonomic ganglia: synaptic pathology as a common theme in neuropathology. Adv. Pathol. Lab. Med. 6, 505–522.

Seitelberger, F., 1986. Neuroaxonal dystrophy: its relation to aging and neurological diseasesVinken, P.J., Bruyn, G.W., Klawans, H.L. (Eds.), Handbook of Clinical Neurology (Vol. vol. 49, Rev. Ser. 5 Elsevier, Amsterdam, pp. 391–415.

Sugimoto, Y., Ninomiya, H., Ohsaki, Y., Higaki, K., Davies, J.P., Ioannou, Y.A., Ohno, K., 2001. Accumulation of cholera toxin and GM1 ganglioside in the early endosome of Nieman–Pick C1-deficient cells. Proc. Natl. Acad. Sci. U. S. A. 98, 12391–12396.

Tanaka, J., Nakamura, H., Miyawaki, S., 1988. Cerebellar involvement in murine sphingomyelinosis: a new model of Nieman–Pick disease. J. Neuropathol. Exp. Neurol. 47, 291–300.

Thomas, P.K., Schaumburg, H.H., Spencer, P.S., Kaeser, H.E., Pallis, C.A., Rose, F.C., Wadia, N.H., 1984. Central distal axonopathy syndromes: newly recognized models of naturally occurring human degenerative disease. Ann. Neurol. 15, 313–314.

Vanier, M.T., Suzuki, K., 1998. Recent advances in elucidating Niemann–Pick disease. Brain Pathol. 8, 163–174.

Webster, K.E., Kemplay, S.K., 1978. Distribution of primary afferent fibres from the forelimb of rat to the upper cervical spinal cord in relation to the location of spinothlamic neuron populations. Neurosci. Lett. 76, 18–24.

Yamada, A., Saji, M., Ukita, Y., Shinoda, Y., Taniguchi, M., Higaki, K., Ninomiya, H., Ohno, K., 2001. Progressive neuronal loss in the ventral posterior lateral and medial nuclei of thalamus in Niemann–Pick disease type C mouse brain. Brain Dev. 23, 288–297.

Zervas, M., Kostantin, K., Walkley, S.U., 2001. Neurons in Niemann–Pick disease type C accumulates gangliosides as well as unesterified cholesterol and undergo dendritic and axonal alterations. J. Neuropathol. Exp. Neurol. 60, 49–64.

Histochem Cell Biol (2004) 121:263–272
DOI 10.1007/s00418-004-0643-7

ORIGINAL PAPER

Yuki Ohsaki · Yuko Sugimoto · Michitaka Suzuki · Toshiyuki Kaidoh · Yukiko Shimada · Yoshiko Ohno-Iwashita · Joanna P. Davies · Yiannis A. Ioannou · Kousaku Ohno · Haruaki Ninomiya

Reduced sensitivity of Niemann-Pick C1-deficient cells to θ-toxin (perfringolysin O): sequestration of toxin to raft-enriched membrane vesicles

Accepted: 16 March 2004 / Published online: 7 April 2004

Abstract θ-Toxin (perfringolysin O) binds to cell surface cholesterol and forms oligomeric pores that cause membrane damage. Both in cytotoxicity and cell survival assays, a mutant Chinese hamster ovary cell line NPC1(−) that lacked Niemann-Pick C1 showed reduced sensitivity to θ-toxin, compared with wild-type (wt) cells. BCθ is a derivative of θ-toxin that retains cholesterol-binding activity but lacks cytotoxicity. Confocal and electron microscopy revealed the presence of multiple vesicles which bound BCθ, both on the cell surface and in the extracellular space of these cells. BCθ binding to raft microdomains was verified by its resistance to 1% Triton X-100 at 4°C and recovery of bound BCθ in floating low-density fractions on sucrose density gradient fractionation. BCθ-labeled vesicles were abolished when NPC1(−) cells were depleted of lipoproteins and also when treated with a Rho-associated kinase inhibitor Y-27632. In addition, similar vesicles were observed in wt cells treated with progesterone. In parallel with these results, θ-toxin sensitivity of NPC1(−) cells was increased when cells were depleted of lipoproteins or treated with Y-27632, whereas that of wt cells was decreased by progesterone. Our findings suggest that sequestration of toxin to raft-enriched cell surface vesicles may underlie reduced sensitivity of NPC1-deficient cells to θ-toxin.

Keywords Cholesterol · Low-density lipoprotein · Progesterone · θ-toxin · Perfringolysin

Y. Ohsaki · Y. Sugimoto · M. Suzuki · H. Ninomiya (✉)
Department of Neurobiology,
Tottori University Faculty of Medicine,
683-8503 Yonago, Japan
e-mail: ninomiya@grape.med.tottori-u.ac.jp
Tel.: +81-859-348276
Fax: +81-859-348135

T. Kaidoh
Department of Anatomy,
Tottori University Faculty of Medicine,
683-8503 Yonago, Japan

Y. Shimada · Y. Ohno-Iwashita
Biomembrane Research Group,
Tokyo Metropolitan Institute of Gerontology,
173-0015 Tokyo, Japan

J. P. Davies · Y. A. Ioannou
Department of Human Genetics,
Mount Sinai School of Medicine,
New York, NY10029, USA

K. Ohno
Department of Child Neurology,
Tottori University Faculty of Medicine,
683-8503 Yonago, Japan

Introduction

Niemann-Pick disease type C (NPC) is an autosomal recessive lipid storage disorder characterized by progressive neurodegeneration, hepatosplenomegaly, and premature death (Vanier and Suzuki 1998). The major complementation group of this disease is caused by mutations in the *NPC1* gene (Carstea et al. 1997). The gene product NPC1 is a mammalian homologue of a resistance-nodulation-division family of prokaryotic permease that primarily resides in the late endosome (Higgins et al. 1999; Davies et al. 2000). NPC1 plays a critical role in intracellular cholesterol transport and the most prominent phenotype of NPC cells is free cholesterol accumulation in the late endosomal/lysosomal system, which is caused by impaired transport of low-density lipoprotein (LDL)-derived cholesterol from these compartments to other cellular sites such as the plasma membrane and the endoplasmic reticulum (Ory 2000).

Besides endosomal accumulation, several lines of evidence suggested alterations in the content/distribution of cell surface cholesterol in NPC cells. First, plasma

membrane fluidity is critically influenced by cholesterol content and it was reduced in NPC human fibroblasts (Koike et al. 1998). Second, cholesterol is the major constituent of cell surface rafts, including caveolae, and both NPC heterozygous human fibroblasts and mouse liver contained high protein levels of caveolin-1 (Garver et al. 1997a, b). Third, NPC cells had reduced sensitivity to the cytotoxicity of cholesterol-binding polyene antibiotics filipin and amphotericin B (Ohno et al. 1993; Higaki et al. 2001). Given the critical roles of cell surface rafts in diverse cellular functions (Simons and Ikonen 1997), alterations in content/distribution of cholesterol at the cell surface may be pertinent to NPC pathology. However, it has not been defined how cell surface cholesterol is altered in NPC cells. Specifically, it is not known how these cells acquire resistance to cholesterol-binding cytotoxins.

θ-Toxin (perfringolysin O), a thiol-activated cytolysin produced by *Clostridium perfringens*, is a protein that binds to membrane cholesterol (Ohno-Iwashita et al. 1991, 1992) and forms oligomeric pores that cause membrane damage (Billington et al. 2000). θ-Toxin digested with subtilisin Carlsberg protease (Cθ) lacks the capacity for oligomerization and hemolytic activity below 20°C (Ohno-Iwashita et al. 1988). Biotinylated Cθ (BCθ) has the same binding affinity to membrane cholesterol as θ-toxin and Cθ but possesses no hemolytic activity even at 37°C (Iwamoto et al. 1997). BCθ has been shown to bind to cholesterol in membrane microdomains that fulfill the biochemical criteria of rafts (Waheed et al. 2001) and has been used as a cytochemical probe to evaluate the topology and distribution of cell surface rafts in intact cells (Fujimoto et al. 1997; Hagiwara et al. 1999; Möbius et al. 2002). BCθ was also used as a probe to visualize intracellular cholesterol accumulation in NPC cells (Sugii et al. 2003) and mouse brains (Reid et al. 2004) under conditions in which cells or tissue sections were fixed and became permeable to this toxin.

The initial purpose of the current studies was to examine whether NPC cells had any alteration in their sensitivity to θ-toxin cytotoxicity. Since we found reduced sensitivity of these cells, we went on to explore an underlying mechanism by using BCθ as a probe. For our purpose, both θ-toxin and BCθ were applied to unfixed, live cells in the current studies.

Materials and methods

Materials

Filipin, methyl-β-cyclodextrin (MβCD), human LDL, and lipoprotein-deficient serum (LPDS) were obtained from Sigma. Progesterone was from ICN Biomedicals. Cholesteryl oleate [cholesteryl-4-^{14}C], ([^{14}C]-CE, 50 Ci/mmol) was from American Radiolabeled Chemicals. Y-27632, lactate dehydrogenase (LDH) cytotoxicity assay kits, and MTT (3-(4,5-dimethylthiazol-2-yl)-2,5-diphenyltetrazolium bromide) cell survival assay kits were from Wako (Tokyo, Japan).

Preparation of θ-toxin and its derivatives

θ-Toxin was expressed in *E. coli*, purified, and the cytotoxic activity of each batch was determined by a hemolysis assay as described (Shimada et al. 1999). θ-Toxin was digested with subtilisin Carlsberg to yield Cθ and then biotinylated to yield BCθ (Iwamoto et al. 1997).

Cell culture

NPC1(−) is a Chinese hamster ovary (CHO) cell line that does not express any NPC1 protein (Higaki et al. 2001). "Knock in" cells were a derivative of NPC1(−) cells that stably expressed wild-type (wt) human NPC1 (Sugimoto et al. 2001). All cells were maintained in Ham's F12/10% bovine calf serum (BCS) at 37°C in a humidified atmosphere containing 5% CO_2. Human skin fibroblasts were cultured as described (Yamamoto et al. 2000).

Cytotoxicity and cell survival assays

Cells in 96-well plates were incubated with θ-toxin in serum-free F12/25 mM HEPES pH 7.4/0.01% bovine serum albumin (BSA). Cytotoxicity in short-term incubations (<30 min) was assessed by LDH activity released into the medium using an LDH assay kit. The medium was filtered through 0.22-μm-pore filters and subjected to the assay. Cell viability in long-term incubations (up to 24 h) was assessed by mitochondrial MTT conversion using an MTT cell survival assay kit.

Microscopy

Cells were washed with PBS and incubated for 30 min at 4°C with 10 μg/ml BCθ in binding buffer (F12/25 mM HEPES pH 7.4/0.01% BSA). For confocal microscopy, BCθ-labeled cells were washed, fixed with PBS/4% paraformaldehyde and incubated for 1 h with 10 μg/ml FITC-avidin. Cells were counterstained with propidium iodide or Texas red-phalloidin as described (Okazawa et al. 1998; Sugimoto et al. 2001) and fluorescent images were obtained with a BioRad MRC1024 confocal microscope. Filipin staining was conducted as described (Higaki et al. 2001) and images were obtained with a Nikon fluorescence microscope.

For scanning electron microscopy, cells were fixed with PBS/3% glutaraldehyde and with 1% osmium tetroxide. After conductive staining with 1% tannic acid/1% osmium tetroxide, they were dehydrated in graded ethanol and critical-point dried with liquid carbon dioxide. The dried specimens were sputter-coated with platinum and examined with an S-4500 Hitachi SEM at 15 kV. For transmission electron microscopy, BCθ-labeled cells were fixed with PBS/4% paraformaldehyde/0.1% glutaraldehyde. After washing, bound toxin was visualized by using an Elite ABC kit (Vector) and DAB. Cells were further fixed with 3% glutaraldehyde and with 1% osmium tetroxide, dehydrated in graded ethanol, and embedded in Epon. Thin sections were stained with lead citrate prior to examination using a Hitachi H-7100 electron microscope at 75 kV.

Sucrose gradient fractionation

Fractionation was performed as described (Waheed et al. 2001) with minor modifications. After BCθ binding, cells were recovered by scraping in 1% Triton X-100/TRIS-buffered saline (TBS; 25 mM TRIS-HCl pH 7.4, 150 mM NaCl, 5 mM EDTA) and homogenized by using a Teflon homogenizer. Homogenates were adjusted to 40% sucrose (w/v), overlaid with 2.4 ml 35% sucrose and 1.3 ml 5% sucrose in TBS, and centrifuged at 250,000 *g* for 18 h at 4°C in an SW50 rotor. A total of eleven 0.4-ml fractions were collected from the top. The pellet was suspended in 0.4 ml TBS and designated as 12th fraction. Proteins in each fraction were

separated by 10% SDS-PAGE and transferred to a PVDF membrane. BCθ was detected using an Elite ABC kit (Vector) and an ECL system (Amersham). For determination of free cholesterol content in each fraction, total lipids were extracted in chloroform/methanol (2:1 v/v), and cholesterol content was measured using a cholesterol assay kit (Molecular Probes). In brief, the extracts were mixed with a reaction mixture containing cholesterol oxidase, horseradish peroxidase, and 10-acetyl-3,7-dihydroxyphenoxazine (Amplex red). In this reaction, H_2O_2 generated by oxidation of cholesterol reacts with Amplex red to yield resorufin. Fluorescence of resorufin was determined by a fluorescence microplate reader.

[^{14}C]-CE LDL labeling and thin-layer chromatography (TLC)

[^{14}C]-CE LDL was prepared as described (Lusa et al. 2001). To maximize LDL incorporation, cells were cultured in LPDS for 3 days and treated with compactin (50 μM; Sankyo, Tokyo, Japan) for 6 h. The sterol-deprived cells were incubated for 16 h with [^{14}C]-CE LDL (50 μg/ml, 10^6 cpm/ml) in F12/10% LPDS, and then chased for 24 h in F12/10% BCS. Extracellular vesicle fractions from [^{14}C]-CE LDL-loaded cells were prepared as described (Dolo et al. 2000). Briefly, culture medium was harvested, centrifuged at 4°C at 300 *g* for 20 min, and then at 1,500 *g* for 30 min to eliminate cell debris. The supernatant was centrifuged twice at 150,000 *g* for 1 h and the final pellet was resuspended in PBS. Total lipids were extracted from cells and extracellular vesicle fractions and were analyzed by TLC as described (Sugimoto et al. 2001). Briefly, lipids were extracted in chloroform/methanol (2:1 v/v) and separated on Silica Gel 60 (Merck) in hexane/diisopropylether/acetic acid (65:35:2 v/v/v) and the autoradiograph was developed with BAS 2000 (Fujitsu, Tokyo).

Results

Reduced sensitivity of NPC1(−) cells to θ-toxin cytotoxicity

We examined cellular sensitivity to θ-toxin by using two assays, an LDH release assay and an MTT conversion assay. In short-term exposures to the toxin up to 30 min, the amounts of LDH released into the medium were lower in NPC1(−) than in wt cells (Fig. 1a), suggesting reduced sensitivity of NPC1(−) cells. This was confirmed by an MTT assay that evaluated cell viability in long-term exposures to the toxin up to 24 h; compared with wt cells, NPC1(−) cells retained statistically higher viability at the toxin concentration of 0.1 HU/ml (Fig. 1b).

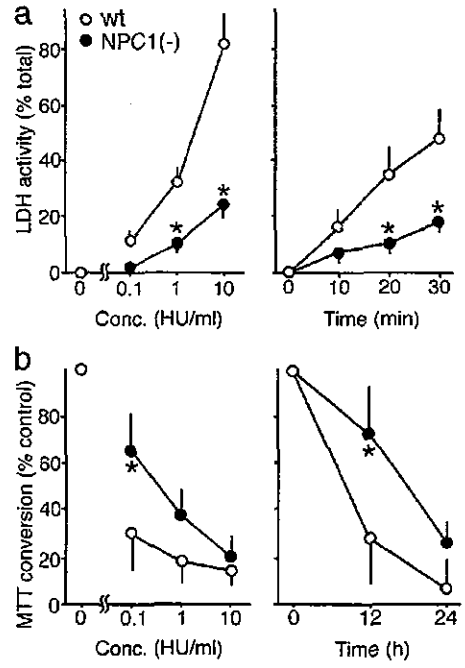

Fig. 1a, b Sensitivity of Chinese hamster ovary cells to θ-toxin cytotoxicity. **a** Lactate dehydrogenase (*LDH*) release assay. The reaction time was 20 min in dose-response experiments (*left*) and the concentration of θ-toxin was 1 HU/ml in time course experiments (*right*). Values were expressed as relative to the values from cells lysed with 1% Tween 20. **b** MTT cell survival assay. The reaction time was 12 h (*left*) and the concentration was 0.1 HU/ml (*right*). Values were expressed as relative to the values from untreated cells. Each point represents the mean±SEM of three determinations each done in triplicate. * $P<0.05$, significantly different from the values of wt cells. *NPC1* Niemann-Pick C1, *wt* wild-type

BCθ binding to cell surface vesicles of NPC1(−) cells

Given the difference in θ-toxin sensitivity, we examined the binding of BCθ. When wt cells were incubated with BCθ at 4°C for 30 min, bound BCθ was distributed in an irregular pattern on the cell surface with some toxin concentrated in tiny patches. The distribution was quite different in NPC1(−) cells, and BCθ was detected on multiple large speckles. As a control, these BCθ-labeled speckles were absent in "knock in" cells that stably expressed NPC1 (Fig. 2a). At a higher magnification, some of the speckles formed a ring-like structure and appeared to protrude from the cell surface (Fig. 2b). Cell surface binding of BCθ was clearly seen in a vertical scan image of the cells counterstained with Texas red-phalloidin, which showed a partial overlap between signals from bound BCθ and those from cortical actin filaments (Fig. 2c). Similar patterns were observed when cells were incubated with BCθ at room temperature or 37°C, and there were no obvious signals from intracellular structures in either condition (data not shown).

To examine whether this BCθ-labeling pattern was a common feature of NPC cells, we repeated the labeling experiments using cultured skin fibroblasts from an NPC patient, UCH, which do not express any NPC1 protein (Yamamoto et al. 2000). Again, BCθ was found on multiple speckles at the surface of UCH cells, and as in NPC1(−) cells, some of these speckles formed ring-like structures when observed at a higher magnification, and partially colocalized with signals from cortical actin filaments (data not shown). These BCθ-positive speckles were absent in control cells (Fig. 2d).

Next we characterized BCθ binding by electron microscopy. Scanning electron microscopy revealed the presence of a large number of cell surface vesicles on NPC1(−) cells with a diameter of 0.2–1 μm. Similar clusters of cell surface vesicles were also found in wt cells but in smaller numbers than in NPC1(−) cells (Fig. 2e). Because these vesicles were also present on cells processed without prior BCθ binding (data not shown), their

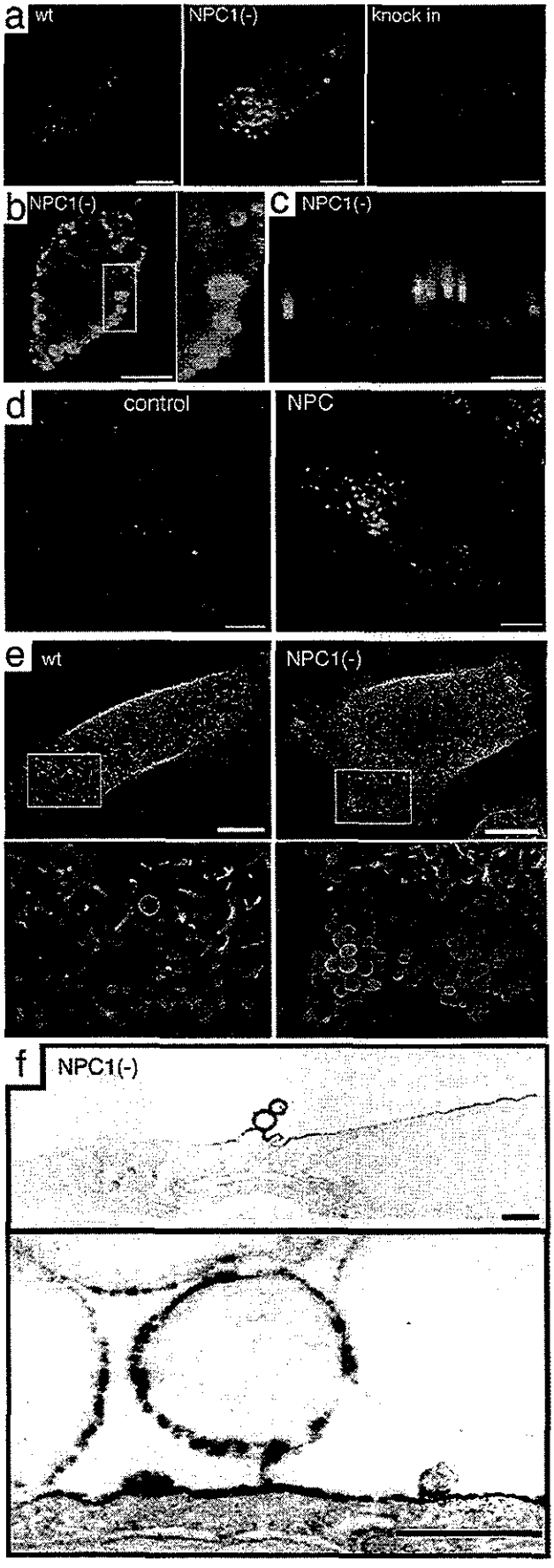

formation was not secondary to toxin binding. Transmission electron microscopy showed localization of bound BCθ on the cell surface vesicles and the juxtapositional plasma membrane (Fig. 2f *upper panel*). Some of the BCθ-labeled vesicles appeared to be detached from the plasma membrane and were found in the extracellular space (Fig. 2f *lower panel*). No signal was detectable in control samples processed without BCθ (data not shown).

Increased levels of BCθ in floating low-density fractions of NPC1(−) cells

Biochemically, raft microdomains are characterized by insolubility in Triton X-100 at cold and by recovery in floating low-density fractions on sucrose gradient fractionation (Simons and Ikonen 1997). To verify BCθ binding to raft microdomains in CHO cells, homogenates were prepared from BCθ-labeled cells in 1% Triton X-100 at 4°C and then fractionated on a sucrose density gradient. BCθ bound to wt cells was recovered in two components. The first component with high buoyancy resided in fractions #4–5 and the second with low buoyancy in bottom fractions #10–12, indicating that at least a part of bound BCθ was recovered in floating low-density fractions. The total amount of BCθ recovered from NPC1(−) cells was higher than that from wt cells. On fractionation, there were increased levels of BCθ in fractions #3 and #4, with a concomitant decrease in the levels of the bottom fractions. Thus in NPC1(−) cells, bound BCθ was more preferentially recovered in floating low-density fractions, and within these fractions appeared to be localized in fractions with higher buoyancy (Fig. 3a).

To verify BCθ binding to cholesterol, we tested effects of MβCD which extracts cell surface cholesterol. Both in wt and NPC1(−) cells, treatment of cells with MβCD (2 mM for 30 min) prior to BCθ binding totally abolished the recovery of BCθ in floating low-density fractions and also reduced the levels in bottom fractions, thus diminishing the differences between the two cell lines (Fig. 3a). To confirm that these MβCD effects were secondary to cholesterol depletion, we determined free cholesterol content in each fraction. Total free cholesterol contents were 73±2 and 124±7 mg/mg protein in wt and NPC1(−)

Fig. 2a–f Biotinylated θ-toxin nicked with subtilisin Carlsberg protease (BCθ) binding to live cells. **a–d** Detection by confocal microscopy. Cells were incubated for 30 min at 4°C with 10 μg/ml BCθ, fixed, and counterstained with propidium iodide (**a**, **b**, **d**) or Texas red-phalloidin (**c**). Bound BCθ was visualized with FITC-avidin. **b** BCθ-labeled structures in the *rectangular area* (*left*) are shown enlarged on the *right*. **c** Vertical scan image. **d** Images of human skin fibroblasts from a control subject and an NPC patient UCH. *Bar* 10 μm. **e** Scanning electron microscopy. Enlarged images of the *rectangular areas in upper panels* are shown in *lower panels*. *Bar* 10 μm. **f** Transmission electron microscopy. Bound BCθ was visualized by high electron densities of osmified DAB. Shown are the representative images of BCθ-labeled vesicles. *Bar* 0.5 μm

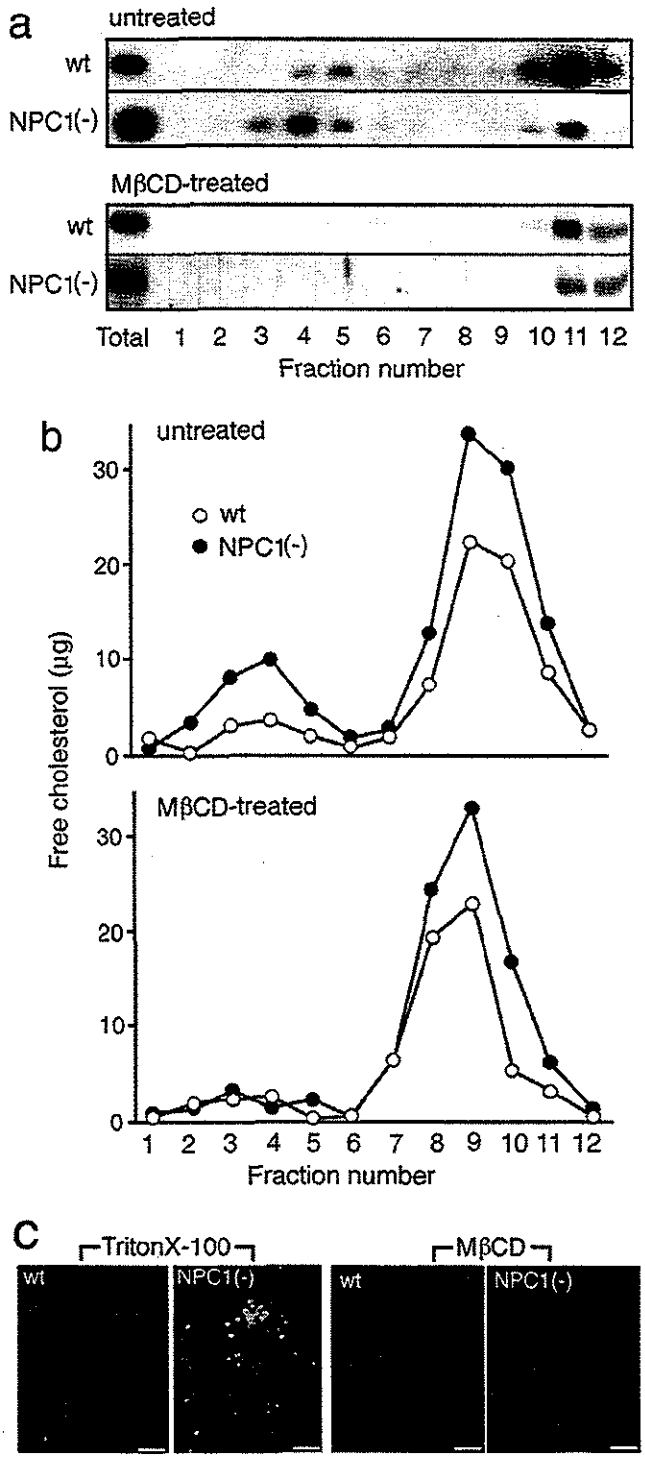

Fig. 3a–c Sucrose gradient fractionation of cell homogenates. **a, b** Cells were treated with or without methyl-β-cyclodextrin (*MβCD*; 2 mM for 30 min) and labeled with BCθ as indicated in the legend to Fig. 2. Cell homogenates prepared in TBS/1% Triton X-100 were subjected to a sucrose density centrifugation and fractionated from the top. Levels of BCθ (**a**) and free cholesterol (**b**) in each fraction were determined. **c** Confocal microscopy. Cells were labeled with BCθ, fixed, and treated with 1% Triton X-100 at 4°C for 30 min or they were treated with MβCD prior to BCθ binding. *Bar* 10 μm

cells, respectively, and these values were reduced to 64±2 and 106±5 mg/mg protein after MβCD treatment (n=3, means±SEM). There were two components that contained relatively high levels of free cholesterol; the first at #2~5 and the second at #7~11. In both components, the levels were higher in NPC1(−) than wt cells. In both cell lines, MβCD treatment decreased the levels in the first component and abolished the difference between the two cell lines. This treatment also caused a shift in the distribution of free cholesterol within the second component; it decreased the levels in #10–11 and increased the levels in #7–8 (Fig. 3b). This shift was observed in both cell lines and the differences in the levels between the two cell lines were not abolished.

Resistance of BCθ binding to Triton X-100 was demonstrated in intact cells; incubation of BCθ-labeled cells with 1% Triton X-100 at 4°C for 30 min caused no discernable changes of the labeling. Effects of MβCD were also demonstrated in intact cells; MβCD treatment caused a decrease in BCθ labeling of both cell lines and completely abolished the labeling of cell surface vesicles in NPC1(−) cells (Fig. 3c).

Suppressed formation of BCθ-labeled vesicles in lipoprotein-depleted NPC1(−) cells

Any alteration in the plasma membrane cholesterol content/distribution of NPC1-deficient cells may be secondary to endosomal free cholesterol accumulation, which can be abolished by culturing cells in LPDS. To see whether the formation of BCθ-labeled vesicles was accompanied by endosomal free cholesterol accumulation, we examined whether these vesicles were present in cells cultured in LPDS. As expected, when NPC1(−) cells were cultured in LPDS for 3 days, their endosomal free cholesterol accumulation was no longer detectable with filipin (Fig. 4a). These cells also lost BCθ-labeled vesicles as revealed by confocal microscopy (Fig. 4b) and scanning electron microscopy (Fig. 4c). Also, there was a clear reduction of BCθ recovered in floating low-density fractions on a sucrose density gradient both in wt and NPC1(−) cells and the difference between the two cell lines was no longer detectable (Fig. 4d).

The absence of BCθ-labeled vesicles in lipoprotein-depleted cells suggested that at least part of the cholesterol contained in these vesicles derived from LDL. To confirm this, we loaded cells with [^{14}C]-CE LDL and examined whether [^{14}C]-labeled free cholesterol ([^{14}C]-FC) was incorporated into extracellular vesicle fractions of the culture medium. In these experiments, cells were first cultured in LPDS and treated with compactin to maximize LDL loading. These lipoprotein-depleted cells were then loaded with [^{14}C]-CE LDL for 16 h, chased in the presence of 10% BCS for 24 h, and harvested for lipid analysis. The chase period was necessary to induce endosomal free cholesterol accumulation in NPC1(−) cells. TLC analysis of cellular lipids showed that there was a marginal increase in the level of [^{14}C]-FC in NPC1(−)

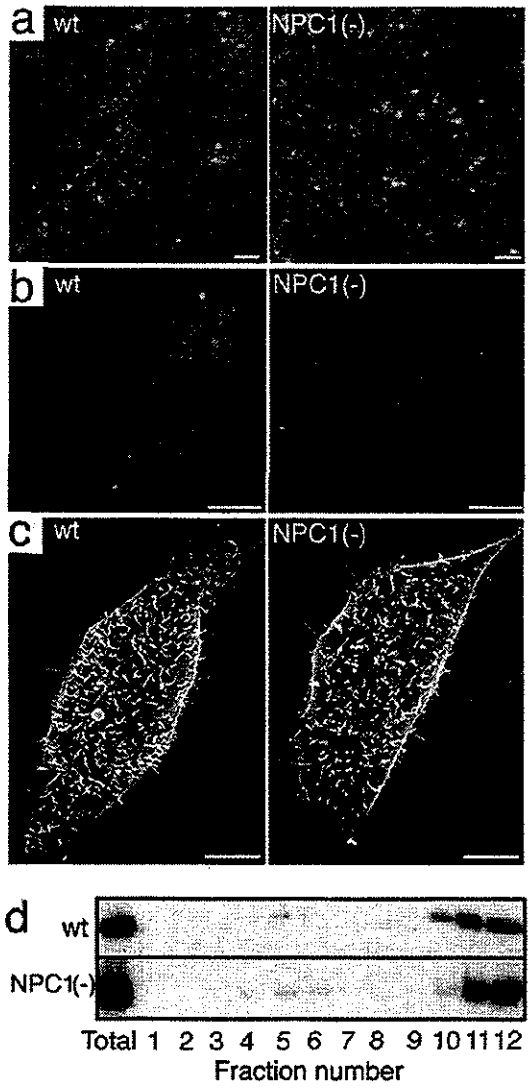

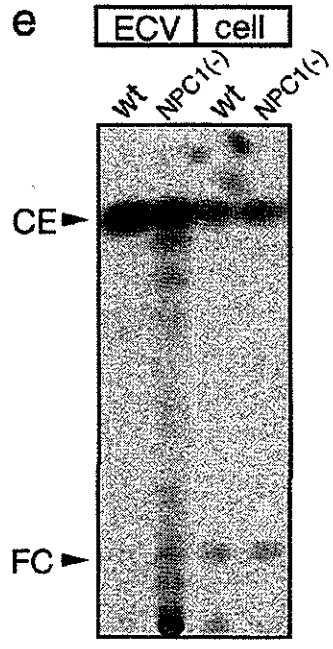

cells compared with that in wt cells. The same analysis of lipids extracted from extracellular vesicle fractions showed the presence of [^{14}C]-FC in these fractions from NPC1(−) cells and its absence in those from wt cells (Fig. 4e).

Formation of BCθ-labeled vesicles in wt cells treated with progesterone

Progesterone inhibits intracellular trafficking of cholesterol and induces NPC-like phenotypes including endosomal free cholesterol accumulation (Butler et al. 1992). We therefore examined whether cell surface vesicles similar to those found in NPC1(−) cells were present in wt cells treated with this compound. When wt cells were cultured with 40 μM progesterone for 24 h, the cells had clear accumulation of free cholesterol in their perinuclear vesicles as revealed by filipin (Fig. 5a). In these progesterone-treated wt cells, BCθ stained multiple speckles on the cell surface as analyzed by confocal microscopy (Fig. 5b). Cell fractionation on a sucrose density gradient revealed increased levels of BCθ recovered in floating low-density fractions of progesterone-treated cells and this increase was accompanied by a decrease in the levels of the bottom fractions. There also was a shift in the distribution of BCθ to a higher buoyancy fraction (#3) within floating low-density fractions (Fig. 5c)

In NPC1(−) cells, progesterone treatment did not affect free cholesterol accumulation (Fig. 5a). Likewise, it did not affect BCθ binding to cell surface vesicles (Fig. 5b). On cell fractionation, it did not change the levels of BCθ recovered in floating low-density fractions #3–4. However, it appeared to increase the levels in fraction #5 as well as the levels in the bottom fractions, as compared with the levels from vehicle-treated cells (Fig. 5c).

Suppressed formation of BCθ-labeled vesicles in NPC1(−) cells treated with Y-27632

Both lipoprotein depletion (Fig. 4) and progesterone treatment (Fig. 5) showed that the formation of BCθ-labeled vesicles was accompanied by endosomal free cholesterol accumulation. We then sought for a method to selectively inhibit the vesicle formation and tested effects

Fig. 4a–e Effects of lipoprotein depletion on the formation of BCθ-labeled vesicles. Cells were cultured in 10% lipoprotein-deficient serum (LPDS) for 3 days. **a** Filipin staining of cells treated with 1% NP-40. **b** Confocal microscopy of BCθ-stained cells. **c** Scanning electron microscopy. **d** Sucrose gradient fractionation. **e** Incorporation of [^{14}C]-labeled free cholesterol ([^{14}C]-FC) derived from [^{14}C]-labeled cholesteryl oleate low-density lipoprotein ([^{14}C]-CE LDL) *into* extracellular vesicle (*ECV*) and cellular fractions. Lipoprotein-depleted cells were loaded with [^{14}C]-CE LDL for 16 h and chased in the presence of 10% bovine calf serum (BCS) for 24 h. Lipid extracts were analyzed by thin-layer chromatography followed by autoradiography. Positions of standard lipids are given (*left*)

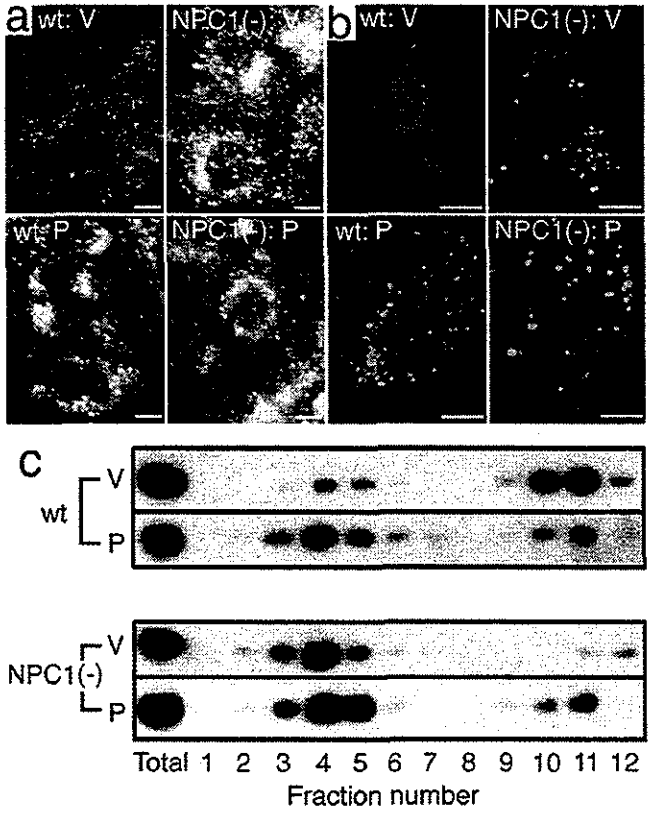

Fig. 5a–c Effects of progesterone on the formation of BCθ-labeled vesicles. Cells were cultured in the presence of 40 μM progesterone (*P*) or vehicle (*V*; 0.1% ethanol) for 24 h before staining with filipin or BCθ. **a** Filipin staining of cells treated with 1% NP-40. **b** Confocal microscopy of BCθ-labeled cells. **c** Sucrose gradient fractionation

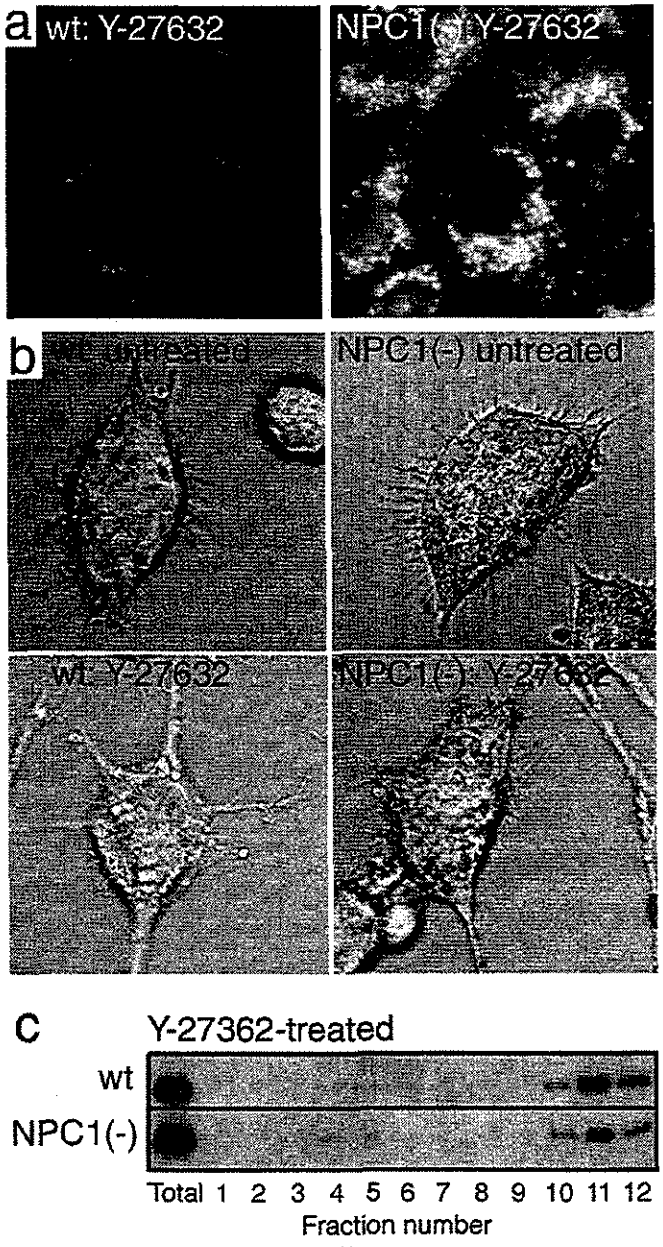

Fig. 6a–c Effects of Y-27632 on the formation of BCθ-labeled vesicles. Cells were cultured in the absence or presence of 15 μM Y-27632 for 24 h and stained with filipin or BCθ. **a** Filipin staining of cells treated with 1% NP-40. **b** Confocal microscopy of BCθ-labeled cells. Signals from bound BCθ (visualized with FITC-avidin) were imposed on differential interference contrast images. **c** Sucrose gradient fractionation

of a Rho-associated kinase inhibitor Y-27632, which disrupts rearrangement of cortical actin filaments (Uehata et al. 1997). This idea originated from partial colocalization of signals from bound BCθ and those from cortical actin filaments (Fig. 2c) and from morphological resemblance of cell surface vesicles to blebs of apoptotic cells, formation of which could be suppressed by this compound (Coleman et al. 2001). Although NPC1(−) cells were never undergoing apoptosis as evidenced by negative staining with FITC-annexin-V and normal nuclear staining with Hoechst (data not shown), we reasoned that rearrangement of cortical actin filaments was also required for the formation of cell surface vesicles.

When cells were treated with Y-27632 at 15 μM for 24 h, they lost short and thin foot-like processes and instead protruded long and thick cytoplasmic extensions as shown in differential interference contrast images (Fig. 6b). These changes most likely resulted from cytoskeletal reorganization and were observed both in wt and NPC1(−) cells. This treatment caused no discernable changes in intracellular cholesterol accumulation as revealed by filipin staining (Fig. 6a). However, the same treatment abolished BCθ binding to NPC1(−) cells (Fig. 6b) and also caused a clear reduction of BCθ recovered in floating low-density fractions on a sucrose density gradient (Fig. 6c).

Correlation between cell surface vesicle formation and θ-toxin sensitivity

To examine whether the formation of cell surface vesicles correlated with cellular sensitivity to θ-toxin, we examined the effects of lipoprotein depletion, progesterone,

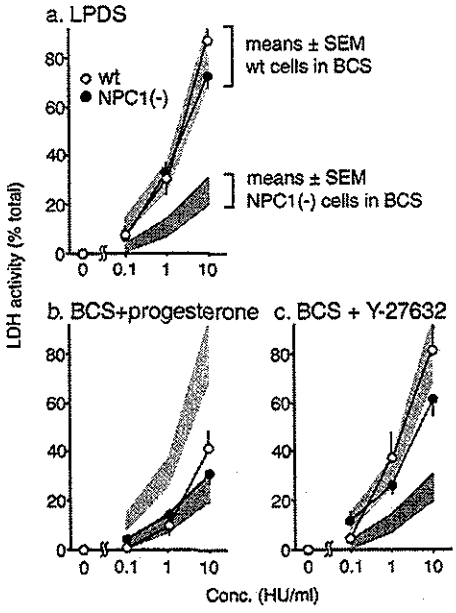

Fig. 7a–c Effects of lipoprotein-depletion, progesterone, and Y-27632 on cellular sensitivity to θ-toxin. Cells were cultured in LPDS for 3 days (**a**) or they were cultured in BCS in the presence of progesterone (40 μM for 24 h; **b**) or Y-27632 (15 μM for 24 h; **c**). LDH release assay was conducted as described in the legend to Fig. 1. The reaction time was 20 min. The vehicle for progesterone (0.1% ethanol) did not affect LDH release (data not shown). For comparison, the mean±SEM ranges of values from cells cultured in BCS without drugs (shown in Fig. 1a) were superimposed in each graph. Each point represents the mean±SEM of three determinations each done in triplicate. There were no statistical differences between the values from wt and NPC1(−) cells in either condition

and Y-27632 on LDH release from cells exposed to θ-toxin.

When cells were cultured in LPDS for 3 days and then exposed to θ-toxin, the amounts of LDH released were increased in NPC1(−) cells as compared with the values from cells cultured in normal serum. The release from wt cells was barely affected by lipoprotein depletion and the difference between the two cell lines was no longer detectable (Fig. 7a). In contrast, progesterone treatment (40 μM for 24 h) resulted in a decrease of the release in wt cells, but not in NPC(−) cells, and again the difference between the two cell lines was abolished (Fig. 7b). Effects of Y-27632 were similar to those of lipoprotein depletion; treatment with this compound (15 μM for 24 h) caused an increase in the release in NPC1(−) cells, but not in wt cells, and abolished the difference between the two cell lines (Fig. 7c).

Discussion

NPC1-deficient cells have been known for their reduced sensitivity to cholesterol-binding cytotoxins such as filipin and amphotericin B and, indeed, our NPC1(−) cells had been selected on their resistance against filipin cytotoxicity (Higaki et al. 2001). Three potential mechanisms had been proposed. First, NPC1-deficient cells may bind a smaller amount of toxin presumably because of a reduced level of cell surface cholesterol, as expected from impaired relocation of endosomal cholesterol. Second, the large intracellular pool of cholesterol in these cells may protect the plasma membrane by taking up bound toxin. Third, a localized change in lipid content/composition may interfere with pore-forming capacities of these toxins (De Kruijff 1990; Jacobs et al. 1997; Liscum and Munn 1999; Lang et al. 2002).

NPC1(−) cells also had reduced sensitivity to θ-toxin (Fig. 1) and results from BCθ binding assays gave some insights to an underlying mechanism. First, NPC1(−) cells had rather increased levels of a cell surface BCθ binding capacity as analyzed by confocal imaging (Fig. 2) and cell fractionation (Fig. 3), excluding that the reduced sensitivity was due to a reduction in the toxin-binding capacity. Second, since NPC1(−) cells did not internalize bound toxin, it was unlikely that the reduced sensitivity was due to sequestration of toxin to an intracellular cholesterol pool. Preferential binding of BCθ to cell surface membrane vesicles (Fig. 2) lets us propose a novel mechanism that the reduced sensitivity was due to sequestration of toxin to cholesterol-enriched cell surface vesicles. This notion was substantiated by the correlation between the presence of these vesicles and cellular resistance to θ-toxin. When cells possessed these vesicles, as in NPC1(−) cells cultured with normal serum (Fig. 2) or in wt cells treated with progesterone (Fig. 5), they showed reduced sensitivity and in opposite conditions where cells lost these vesicles, as in NPC1(−) cells cultured with LPDS (Fig. 4) or treated with Y-27632 (Fig. 6), they showed higher sensitivity (Fig. 7). By using Y-27632, we were able to suppress vesicle formation and to increase sensitivity of NPC1(−) cells without interfering with endosomal cholesterol accumulation, providing further evidence for independence of cellular sensitivity from an intracellular cholesterol pool.

Given the sequestration of toxin to cell surface vesicles, how could this lead to cellular resistance? One possible explanation is that active shedding of these vesicles resulted in a reduction of toxin on the remaining part of the plasma membrane. This notion copes with the presence of BCθ-labeled vesicles in the extracellular space of NPC1(−) cells (Fig. 2), although we could not demonstrate a localized reduction of toxin in such areas. Alternatively, it is possible that these vesicles and the juxtapositional plasma membrane had lipid compositions different from other parts of the plasma membrane, and such that θ-toxin oligomerization and/or subsequent pore formation was interfered with in those areas.

Cell fractionation studies revealed increased levels of BCθ recovered in floating low-density fractions of NPC1(−) cells, and there was also a shift in the distribution to higher buoyancy fractions, as compared with the levels and distribution in wt cells (Fig. 3). Notably a similar increase and a shift were induced in wt cells by progesterone (Fig. 5). BCθ bound to cell surface vesicles of NPC1(−) cells was apparently recovered in floating

low-density fractions because of clear reductions in these fractions from cells cultured in LPDS (Fig. 4) or treated with Y-27632 (Fig. 6). Therefore, preferential recovery of BCθ in floating low-density fractions as well as a shift in distribution within these fractions might reflect a difference in lipid compositions between cell surface vesicles and other areas of the plasma membrane, which should be determined by further analyses. In these experiments, effects of progesterone on NPC1(−) cells were paradoxical, as compared with those on wt cells, and it increased the levels of BCθ in fraction #5 that had relatively lower buoyancy within floating low-density fractions as well as the levels in the bottom fractions (Fig. 5). These effects, however, were not accompanied by an alteration in cellular sensitivity to θ-toxin (Fig. 7b) and their biochemical mechanism was left unresolved.

Previous cytochemical studies showed that BCθ-labeled raft microdomains did not evenly distribute on the cell surface but were concentrated in specific regions such as short processes in lymphocytes (Hagiwara et al. 1999) and filopodia/pseudopodia in platelets (Waheed et al. 2001) and lymphoblastoid cells (Möbius et al. 2002). In addition to these regions, Hagiwara et al. (1999) found dense labeling of shed membrane vesicles in lymphocytes labeled with BCθ and FITC-avidin in the live state and, because of its temperature dependence, suggested that these vesicles were formed by crosslinking of cell surface cholesterol by BCθ/avidin complexes. From a morphological point of view, BCθ binding to membrane vesicles of NPC1(−) cells is reminiscent of their finding. However, these vesicles were present in NPC1(−) cells without BCθ labeling as analyzed by scanning electron microscopy, and their formation did not depend on temperature as analyzed by confocal microscopy. In addition, FITC-avidin was applied after fixation of BCθ-labeled cells in our protocol. Although we could not exclude undetectable changes in morphology and/or abundance of these vesicles induced by BCθ labeling, these lines of evidence argue that the presence of these vesicles was an intrinsic feature of NPC1(−) cells.

Implications of our findings in NPC cell pathology remain unclear. However, it is plausible that formation and shedding of raft-enriched membrane vesicles in NPC1(−) cells was caused by a disturbance in cellular cholesterol traffic and hence is supposed to be one of cellular responses to adapt the traffic jam. It was suggested that in NPC cells, LDL-derived cholesterol jammed on the endosomal membrane was packaged in rafts and was transported to multivesicular bodies via intraluminal membrane budding (Lusa et al. 2001). Incorporation of LDL-derived cholesterol into extracellular vesicle fractions of NPC1(−) cells (Fig. 4e) suggested that similar events happened on the plasma membrane where jammed cholesterol was packaged in rafts and was transported to extracellular vesicles. Thus, there may be a common mechanism that operates both on the endosome and the plasma membrane to regulate cholesterol-enriched membrane flow. It is also left unknown how our findings relate to in situ NPC pathology. Cells in solid organs are surrounded by extracellular matrix or other cells and it is unlikely that they release the vesicles as observed in cultured cells. Circulating blood cells may be the primary target to examine whether a similar phenomenon happens in NPC patients or animals.

In summary, we found reduced sensitivity of NPC1-deficient CHO cells to θ-toxin and proposed a novel mechanism that it was due to sequestration of toxin to raft-enriched cell surface vesicles. Detailed mechanisms for the formation of these vesicles and their implications in NPC pathology should be clarified in future studies.

Acknowledgements We thank Drs. S. Sugii and T.Y. Chang for their valuable comments on the manuscript.

References

Billington SJ, Jost BH, Songer JG (2000) Thiol-activated cytolysins: structure, function and role in pathogenesis. FEMS Microbiol Lett 182:197–205

Butler JD, Blanchette-Mackie EJ, Goldin E, O'Neill RR, Carstea G, Roff CF, Patterson MC, Patel S, Comly ME, Cooney A (1992) Progesterone blocks cholesterol translocation from lysosomes. J Biol Chem 267:23797–23805

Carstea ED, Morris JA, Coleman KG, Loftus SK, Zhang D, Cummings C, Gu J, Rosenfeld MA, Pavan WJ, Krizman DB, Nagle J, Polymeropoulos MH, Sturley SL, Ioannou YA, Higgins ME, Comly M, Cooney A, Brown A, Kaneski CR, Blanchette-Mackie EJ, Dwyer NK, Neufeld EB, Chang TY, Liscum L, Strauss JF III, Ohno K, Zeigler M, Karmi R, Sokol J, Markie D, O'Neill RR, van Diggelen OP, Elleder M, Patterson MC, Brady RO, Vanier MT, Pentchev PG, Tagle DA (1997) Niemann-Pick C1 disease gene: homology to mediators of cholesterol homeostasis. Science 277:228–231

Coleman ML, Sahai EA, Yeo M, Bosch M, Dewar A, Olson MF (2001) Membrane blebbing during apoptosis results from caspase-mediated activation of ROCK I. Nat Cell Biol 3:339–345

Davies JP, Chen FW, Ioannou YA (2000) Transmembrane molecular pump activity of Niemann-Pick C1 protein. Science 290:2295–2298

De Kruijff B (1990) Cholesterol as a target for toxins. Biosci Rep 10:127–130

Dolo V, Li R, Dillinger M, Flati S, Manela J, Taylor BJ, Pavan A, Ladisch S (2000) Enrichment and localization of ganglioside G(D3) and caveolin-1 in shed tumor cell membrane vesicles. Biochim Biophys Acta 1486:265–274

Fujimoto T, Hayashi M, Iwamoto M, Ohno-Iwashita Y (1997) Crosslinked plasmalemmal cholesterol is sequestered to caveolae: analysis with a new cytochemical probe. J Histochem Cytochem 45:1197–1205

Garver WS, Erickson RP, Wilson JM, Colton TL, Hossain GS, Kozloski MA, Heidenreich RA (1997a) Altered expression of caveolin-1 and increased cholesterol in detergent insoluble membrane fractions from liver in mice with Niemann-Pick disease type C. Biochim Biophys Acta 1361:272–280

Garver WS, Hsu SC, Erickson RP, Greer WL, Byers DM, Heidenreich RA (1997b) Increased expression of caveolin-1 in heterozygous Niemann-Pick type II human fibroblasts. Biochem Biophys Res Commun 236:189–193

Hagiwara H, Kogure S, Nakamura M, Shimada Y, Ohno-Iwashita Y, Fujimoto T (1999) Cross-linking of plasmalemmal cholesterol in lymphocytes induces capping, membrane shedding, and endocytosis through coated pits. Biochem Biophys Res Commun 260:516–521

Higaki K, Ninomiya H, Sugimoto Y, Suzuki T, Taniguchi M, Niwa, H, Pentchev PG, Vanier MT, Ohno K (2001) Isolation of

NPC1-deficient Chinese hamster ovary cell mutants by gene trap mutagenesis. J Biochem 129:875–880

Higgins ME, Davies JP, Chen FW, Ioannou YA (1999) Niemann-Pick C1 is a late endosome-resident protein that transiently associates with lysosomes and the trans-Golgi network. Mol Genet Metab 68:1–13

Iwamoto M, Morita I, Fukuda M, Murota S, Ando S, Ohono-Iwashita Y (1997) A biotinylated perfringolysin O derivative: a new probe for detection of cell surface cholesterol. Biochim Biophys Acta 1327:222–230

Jacobs NL, Andemariam B, Underwood KW, Panchalingam K, Sternberg D, Kielian M, Liscum L (1997) Analysis of a Chinese hamster ovary cell mutant with defective mobilization of cholesterol from the plasma membrane to the endoplasmic reticulum. J Lipid Res 38:1973–1987

Koike T, Ishida G, Taniguchi M, Higaki K, Ayaki Y, Saito M, Sakakihara Y, Iwamori M, Ohno K (1998) Decreased membrane fluidity and unsaturated fatty acids in Niemann-Pick disease type C fibroblasts. Biochim Biophys Acta 1406:327–335

Lang Y, Ye J, Rigney M, Steck TL (2002) Dynamics of lysosomal cholesterol in Niemann-Pick type C and normal human fibroblasts. J Lipid Res 43:198–204

Liscum L, Munn NJ (1999) Intracellular cholesterol transport. Biochim Biophys Acta 1438:19–37

Lusa S, Blom TS, Eskelinen EL, Kuismanen E, Mansson JE, Ikonen E (2001) Depletion of rafts in late endocytic membranes is controlled by NPC1-dependent recycling of cholesterol to the plasma membrane. J Cell Sci 114:1893–1200

Möbius W, Ohno-Iwashita Y, van Donselaar EG, Oorschot VM, Shimada Y, Fujimoto T, Heijnen HF, Geuze HJ, Slot JW (2002) Immunoelectron microscopic localization of cholesterol using biotinylated and non-cytolytic perfringolysin O. J Histochem Cytochem 50:43–55

Ohno K, Nanba E, Nakano T, Inui K, Okada S, Takeshita K (1993) Altered sensitivities to potential inhibitors of cholesterol biosynthesis in Niemann-Pick type C fibroblasts. Cell Struct Funct 18:231–240

Ohno-Iwashita Y, Iwamoto M, Mitsui K, Ando S, Nagai Y (1988) Protease-nicked θ-toxin of *Clostridium perfringens*, a new membrane probe with no cytolytic effect, reveals two classes of cholesterol as toxin-binding sites on sheep erythrocytes. Eur J Biochem 176:95–101

Ohno-Iwashita Y, Iwamoto M, Mitsui K, Ando S, Iwashita S (1991) A cytolysin, θ-toxin, preferentially binds to membrane cholesterol surrounded by phospholipids with 18-carbon hydrocarbon chains in cholesterol-rich region. J Biochem 110:369–375

Ohno-Iwashita Y, Iwamoto M, Ando S, Iwashita S (1992) Effect of *lipidic factors* on membrane cholesterol topology: mode of binding of θ-toxin to cholesterol in liposomes. Biochim Biophys Acta 1109:81–90

Okazawa M, Shiraki T, Ninomiya H, Kobayashi S, Masaki T (1998) Endothelin-induced apoptosis of A375 human melanoma cells. J Biol Chem 273:12584–12592

Ory DS (2000) Niemann-Pick type C: a disorder of cellular cholesterol trafficking. Biochim Biophys Acta 1529:331–339

Reid PC, Sakashita N, Sugii S, Ohno-Iwashita Y, Shimada Y, Hickey WF, Chang TY (2004) A novel cholesterol stain reveals early neuronal cholesterol accumulation in the *Niemann*-Pick type C1 mouse brain. J Lipid Res (Epub ahead of print)

Shimada Y, Nakamura M, Naito Y, Nomura K, Ohno-Iwashita Y (1999) C-terminal amino acid residues are required for the folding and cholesterol binding property of perfringolysin O, a pore-forming cytolysin. J Biol Chem 274:18536–18542

Simons K, Ikonen E (1997) Functional rafts in cell membranes. Nature 387:569–572

Sugii S, Reid PC, Ohgami N, Shimada Y, Maue RA, Ninomiya H, Ohno-Iwashita Y, Chang TY (2003) Biotinylated θ-toxin derivative as a probe to examine intracellular cholesterol-rich domains in normal and Niemann-Pick type C1 cells. J Lipid Res 44:1033–1041

Sugimoto Y, Ninomiya H, Ohsaki Y, Higaki K, Davies JP, Ioannou YA, Ohno K (2001) Accumulation of cholera toxin and GM1 ganglioside in the early endosome of Niemann-Pick C1-deficient cells. Proc Natl Acad Sci U S A 98:12391–12396

Uehata M, Ishizaki T, Satoh H, Ono T, Kawahara T, Morishita T, Tamakawa H, Yamagami K, Inui J, Maekawa M, Narumiya S (1997) Calcium sensitization of smooth muscle mediated by a Rho-associated protein kinase in hypertension. Nature 389: 990–994

Vanier MT, Suzuki K (1998) Recent advances in elucidating Niemann-Pick C disease. Brain Pathol 8:163–174

Waheed AA, Shimada Y, Heijnen HF, Nakamura M, Inomata M, Hayashi M, Iwashita S, Slot JW, Ohno-Iwashita Y (2001) Selective binding of perfringolysin O derivative to cholesterol-rich membrane microdomains (rafts). Proc Natl Acad Sci U S A 98:4926–4931

Yamamoto T, Ninomiya H, Matusmoto M, Ohta Y, Nanba E, Tsutsumi Y, Yamakawa K, Millat G, Vanier MT, Pentchev PG, Ohno K (2000) Genotype-phenotype relationship of Niemann-Pick disease type C: a possible correlation between clinical onset and levels of NPC1 protein in isolated skin fibroblasts. J Med Genet 37:707–712

ELSEVIER

Brain & Development 26 (2004) 245–250

BRAIN & DEVELOPMENT
Official Journal of the Japanese Society of Child Neurology

www.elsevier.com/locate/braindev

Original article

Increased *NPC1* mRNA in skin fibroblasts from Niemann-Pick disease type C patients

Toshiyuki Yamamoto[a,*], Jian-Hua Feng[b,c], Katsumi Higaki[d], Miyako Taniguchi[e], Eiji Nanba[f], Haruaki Ninomiya[g], Kousaku Ohno[c]

[a]*Division of Medical Genetics, Kanagawa Children's Medical Center, 2-138-4 Mutsukawa, Minami-ku, Yokohama 232-8555, Japan*
[b]*Department of Child Neurology, Children Hospital, Zhejiang University, Hangzhou 310003, China*
[c]*Division of Child Neurology, Institute of Neurological Sciences, Faculty of Medicine, Tottori University, Yonago 683-8503, Japan*
[d]*Institute of Human Nutrition, Columbia University College of Physicians and Surgeons, New York, NY 10032, USA*
[e]*Department of Biological Regulation, School of Health Sciences, Faculty of Medicine, Tottori University, Yonago 683-8503, Japan*
[f]*Gene Research Center, Tottori University, Yonago 683-8503, Japan*
[g]*Department of Neurobiology, School of Life Sciences, Faculty of Medicine, Tottori University, Yonago 683-8503, Japan*

Received 18 November 2002; received in revised form 25 May 2003; accepted 24 July 2003

Abstract

Niemann-Pick disease type C (NP-C) is an autosomal recessive lipid-storage disease that is characterized by progressive neurodegeneration and hepatosplenomegaly. Since identification of the *NPC1* gene in 1997, a total of 120 disease-causing mutations have been reported. In this study, two novel mutations were identified, namely c.2508[-2509]A del (837Fs-838X) in exon 16 and T3194G (V1065G) in exon 21. To explore the impact of *NPC1* mutations on transcription of this gene, we analyzed *NPC1* mRNA levels in skin fibroblasts derived from NP-C patients. Fibroblasts from patients with missense mutations showed increased levels of *NPC1* mRNA while fibroblasts from patients with a specific frameshift mutation showed mRNA levels similar to those of normal control subjects. These results suggest that *NPC1* transcription levels are altered in cells with mutations in the *NPC1* gene.

Keywords: *NPC1* mRNA; Niemann-Pick disease type C; Northern blotting; Mutation

1. Introduction

Niemann-Pick disease type C (NP-C; MIM#257220) is a rare autosomal recessive lipid-storage disorder characterized by impaired intracellular cholesterol transport. The incidence of the disease is estimated at about one in 10^5 live births [1]. Affected patients show hepatosplenomegaly (HSM) and neurodegeneration. Neurological symptoms include vertical supranuclear ophthalmoplegia (VSO), progressive ataxia, cataplexy, epilepsy and dementia. According to the onset of these symptoms, the disease is classified into infantile, late infantile, juvenile and adult forms [2]. NP-C cells are characterized by the accumulation of a large amount of unesterified cholesterol in the endosomal/lysosomal (E/L) compartment as a result of impaired movement of cholesterol from the E/L system to the plasma membrane [3]. Somatic cell hybridization experiments with skin fibroblasts from unrelated NP-C patients have demonstrated the existence of a major complementation group comprising >95% of cases, designated NP-C1, and a minor complementation group, designated NP-C2 [4–6].

NPC1, the gene responsible for NP-C in the major complementation group, has been mapped to chromosome 18q11 [7,8]. The NPC1 protein has a sterol-sensing domain and shares significant homology with the morphogen receptor Patched [9]. NPC1 is an integral membrane protein that localizes to the E/L system [10]. The 4.7-kb *NPC1* cDNA contains 25 exons encoding a 1278-amino-acid protein comprising thirteen transmembrane (TM) domains, three large luminal loops, four small luminal

* Corresponding author. Tel.: +81-45-711-2351; fax: +81-45-742-7821.
E-mail address: nikau@basil.freemail.ne.jp (T. Yamamoto).

0387-7604/$ - see front matter © 2003 Elsevier B.V. All rights reserved.
doi:10.1016/S0387-7604(03)00162-1